Collider Events at the LHC

With this introduction to the Standard Model at 100 GeV energies, we are ready to discuss the properties of collision events at the LHC. The most important observation to make is that the rates of LHC physics processes span an enormous range of scales. The cross section for *anything* to happen in a pp collision is of the order of 100 mb. Observed cross sections at the LHC go down to about 1 fb. To observe 1 event of the latter type, it is necessary to reject 10^{14} events of the former type. So it is important to understand the properties of this largest class of events—and of all of the classes one meets down to the rarest ones.

The LHC has four detectors, but, for high momentum transfer processes, the important ones are ATLAS and CMS. Figures 1 and 2 show schematic diagrams of these detectors. They are similar to the OPAL dectector that we saw in lecture 1. However, there are some important differences. Obviously, the detectors are much larger, mainly reflecting the difficulty of bending TeV particles and containing their hadronic and electromagnetic showers. The detectors are more developed in the forward direction, for reasons that I will explain below. And, much more attention is given to the measurement of momentum for very high energy muons, since, as we will see, high-energy leptons are important probes of LHC physics.

In discussing physics processes at the LHC, we might begin with the total cross section. Measurements of the total cross section and the inelastic cross section are shown in Figure 3. The data points on the right with large errors are from cosmic ray experiments. The circles are data from the TOTEM experiment, a detector at very small angles downstream from CMS along the beam line, which measured very forward elastic pp scattering. The forward elastic cross section is required to be quite large, since it is related to the inelastic cross section by the optical theorem. The measured inelastic cross section is about 75 mb, which corresponds to

$$75\,\text{mb} = 0.75\times10^{-25}\,\text{cm}^2 = \pi R^2 \text{ for } R = 1.5\,\text{fm}$$

The charge radius of the proton is 0.9 fm, so, roughly, every time the two protons touch, they interact and liberate quarks and gluons. The growth of the cross section, which seems large on this log scale, is in fact quite mild, going as $\log^2 s$. This growth is associated with the growth of a virtual pion cloud around the proton as seen by the incoming proton.

Typical inelastic events liberate a large number of strongly interacting particles, mainly pions. Most of these particles are produced with small momentum transverse

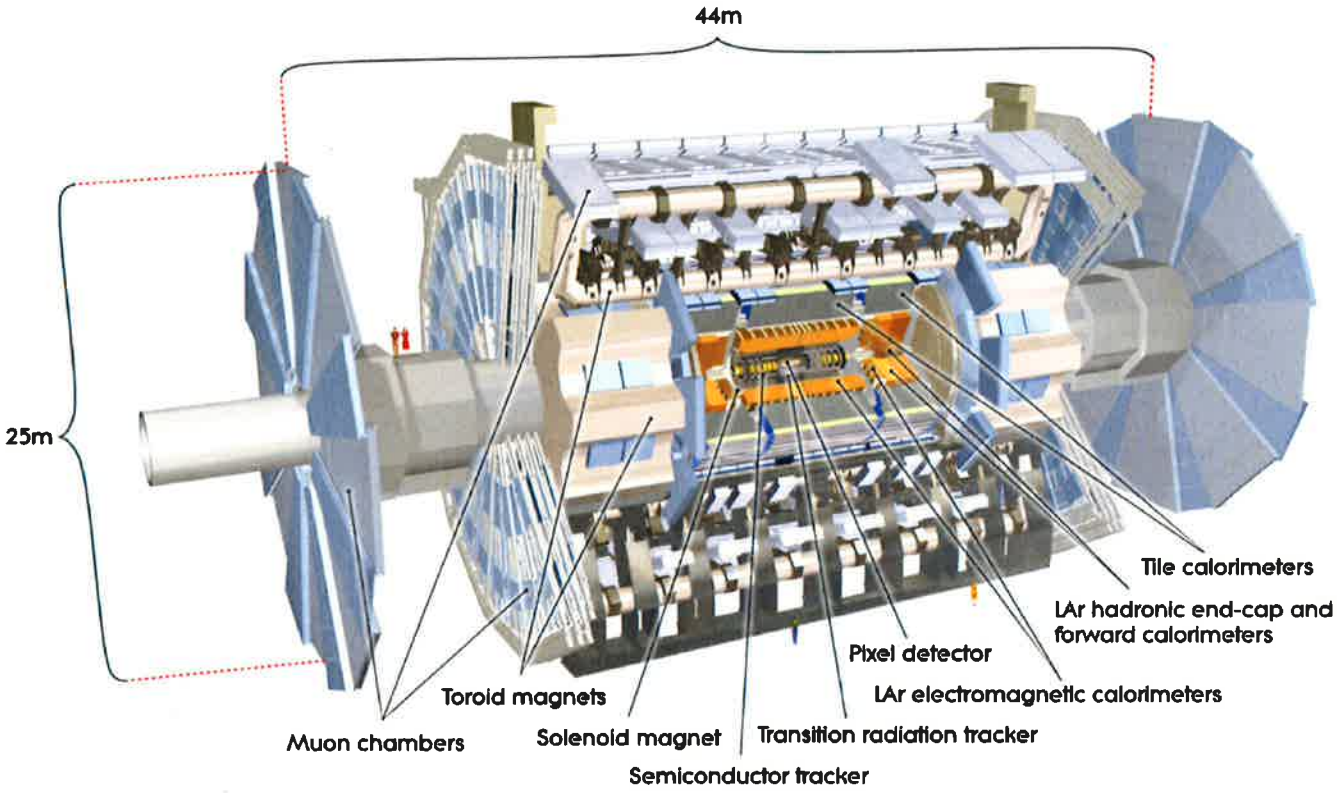

Fig. 1 Schematic Diagram of the ATLAS detector, from ATLAS Collaboration, JINST 3 S08003 (2008).

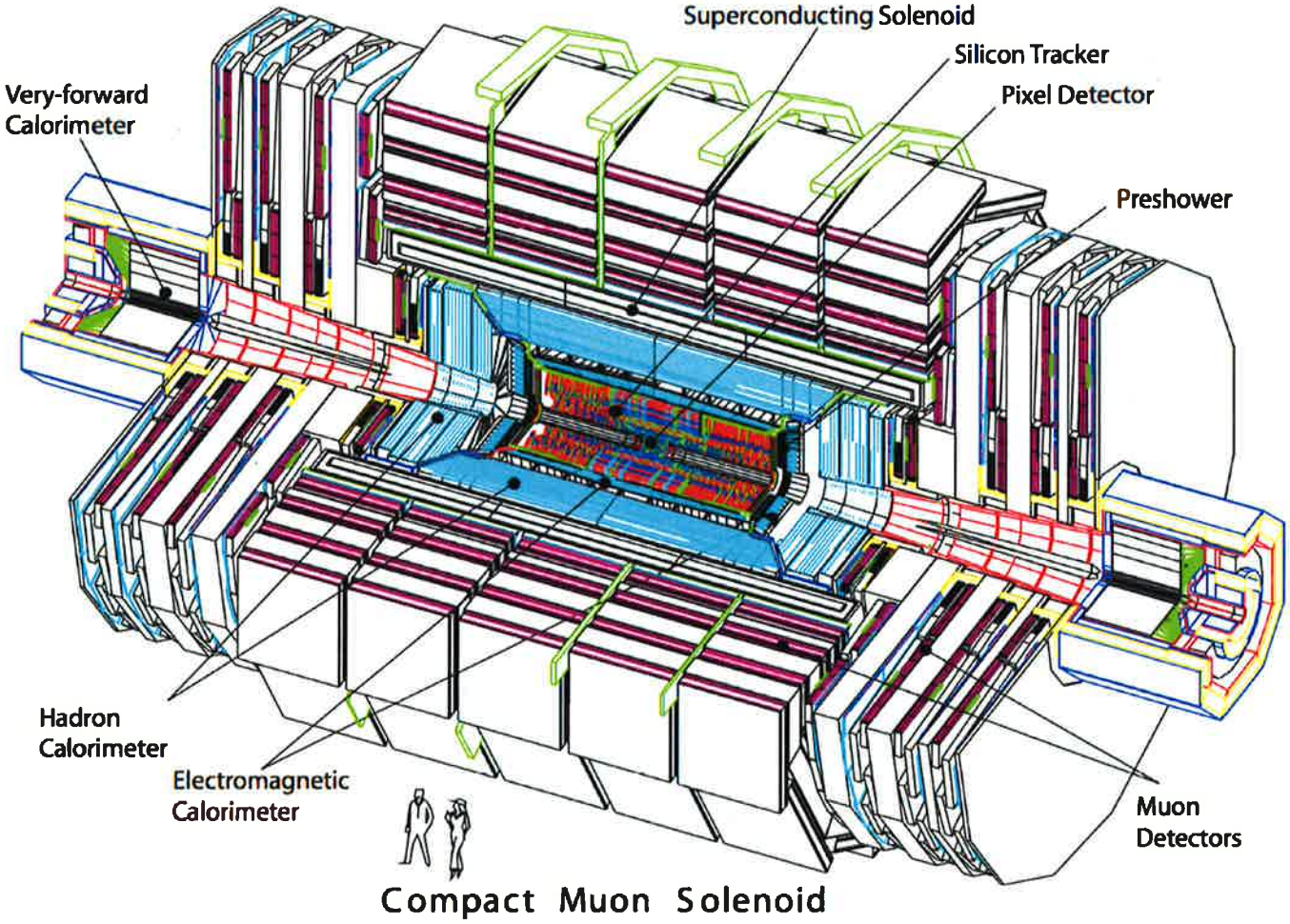

Fig. 2 Schematic diagram of the CMS detector, from CMS Collaboration, JINST 3 S08004 (2008)

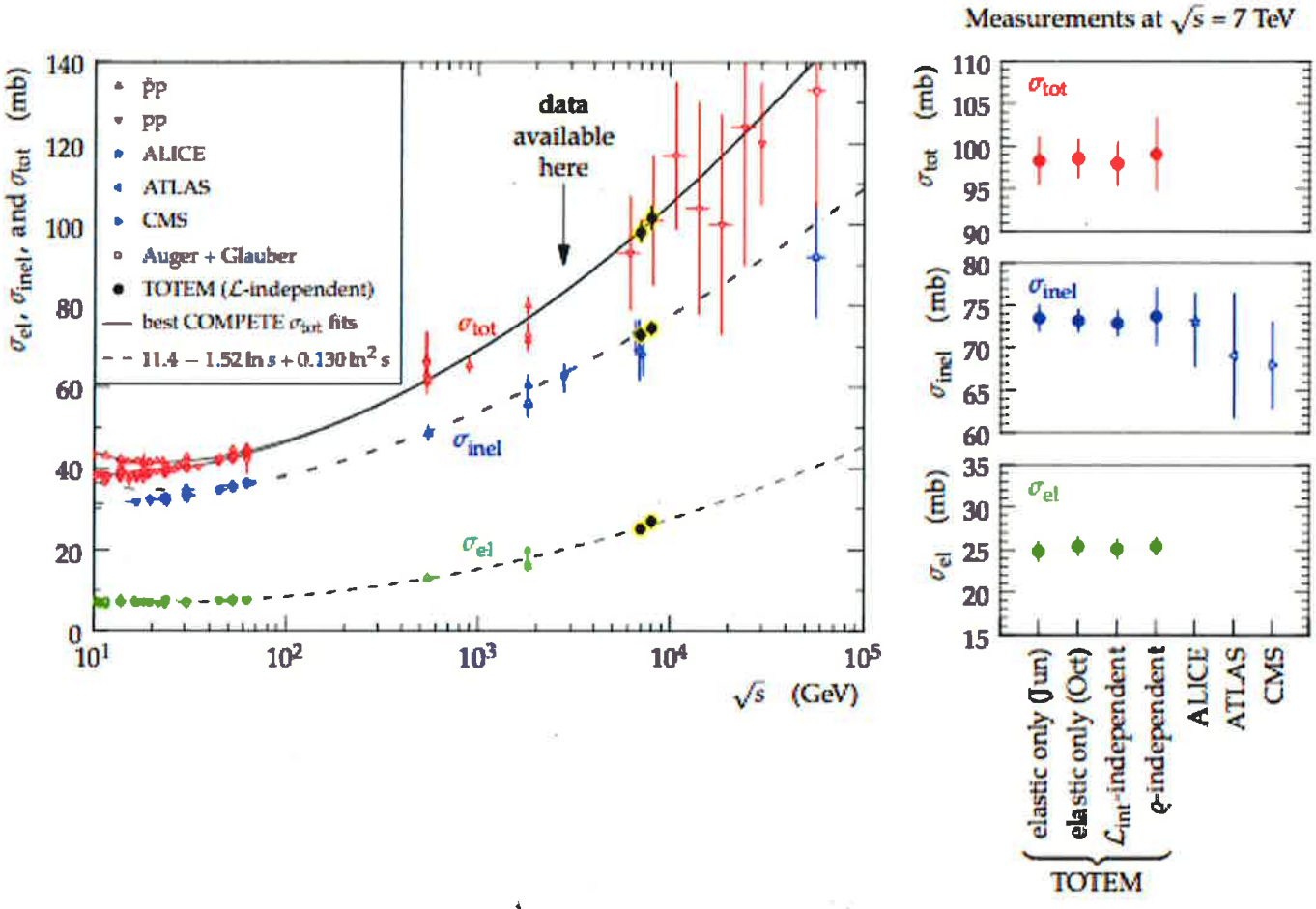

Fig. 3 Measurements of the total and inelastic pp cross sections at high energy, from J Kaspar (TOTEM Collaboration) arXiv 1310.3178.

to the beam direction. The transverse momentum distribution of these particles is shown in Figure 4. This is just as we would expect if large momentum transfer reactions are suppressed by the small value of the QCD coupling at large Q. There are a variety of models of this soft particle production, from models based completely on non-perturbative physics to models based on parton-parton scattering. Both types of models predict that the observed hadrons originate from a range of frames between the rests frames of the two incoming protons. Note that the softly produced particles can have very high energy, as long as their momentum is close to the beam direction.

This dynamic range in longitudinal momentum is most conveniently described using the variable rapidity introduced in lecture 2. Recall that, for a particle with nonzero transverse momentum,

$$p^\mu = m_T (\cosh y, \frac{p_T}{m_T}, \sinh y)$$

where

$$m_T^2 = (p_T^2 + m^2)$$

For pions with transverse momenta above 100 MeV, it makes sense to consider this formula in the limit of zero mass. In this approximation, writing η instead of y, we have

$$p^\mu = p_T (\cosh \eta, 1, \sinh \eta)$$

or

$$e^\eta = \frac{p + p_\parallel}{p_T} = \frac{1+\cos\theta}{\sin\theta} = \left(\frac{1+\cos\theta}{1-\cos\theta}\right)^{\frac{1}{2}}$$

so that

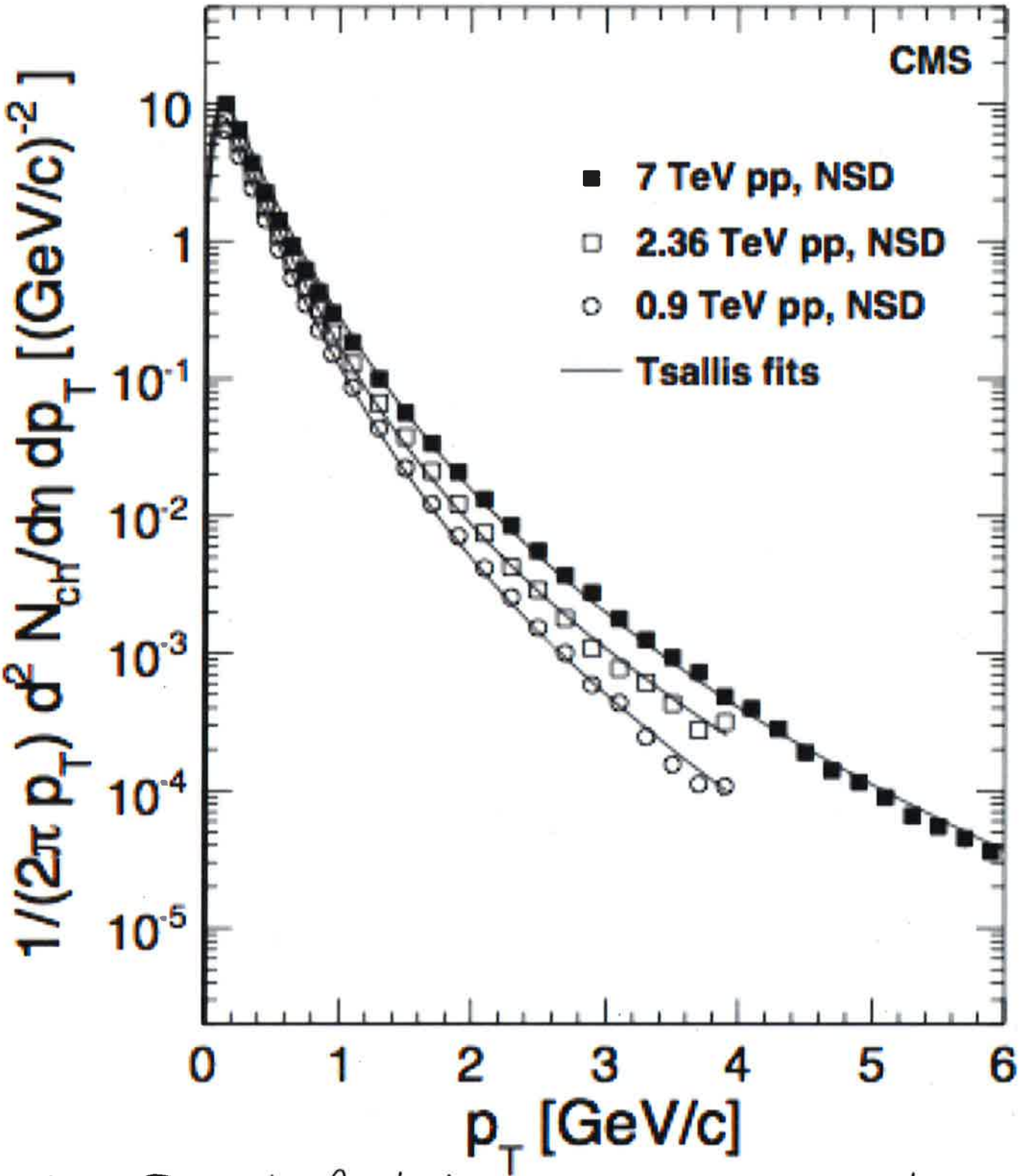

Fig. 4 Distribution of charged hadrons in transverse momentum measured by the CMS Collaboration, arXiv: 1005.3299, Phys. Rev. Lett. 105 022002 (2010).

$$\eta = \frac{1}{2}\log\left(\frac{1+\cos\theta}{1-\cos\theta}\right)$$

The quantity η is called "pseudorapidity". It is a good approximation to rapidity for most produced particles. So it is convenient to use this quantity instead of θ to represent the polar angle in a detector. Since

$$\cos\theta = \frac{e^{2\eta}-1}{e^{2\eta}+1}$$

we can tabulate

η:	θ:
0	90°
1	40.4°
2	15.4°
3	6.7°
4	2.1°
5	0.8°

It becomes very challenging to access rapidities greater than about 4 in a central detector such as ATLAS or CMS. Firgure 5 shows values of pseudorapidity for the CMS detector. There are no tracking elements beyond $\eta = 2.5$, though there is a very forward calorimeter that reaches rapidities above 4.

The rapidity of a beam proton at the 13 TeV LHC is 9.5. It is useful to make a map of rapidity

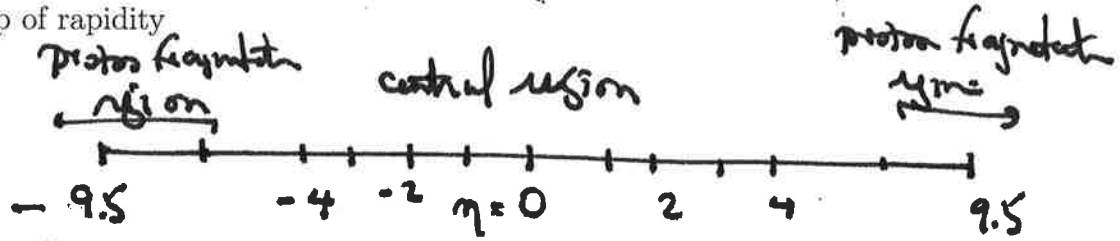

The regions in which particle production is sensitive to the incoming hadrons is called the proton (or other hadron) fragmentation region. At the LHC, it is at very high

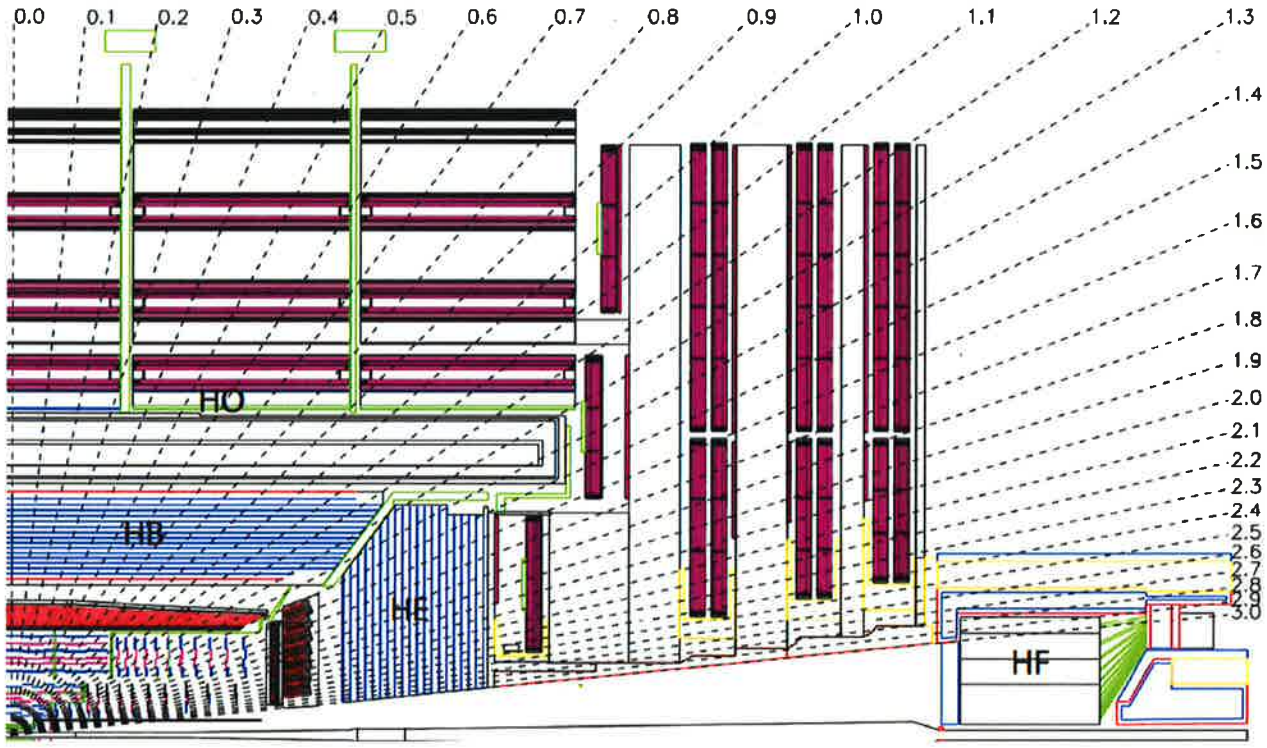

Fig. 5 Layout of the CMS detector in pseudorapidity, from CMS Collaboration JINST 3 S08004 (2008)

rapidity, more or less inaccessible to the detectors. In the central region of rapidity, the particle production is relatively constant. The charged particle production as a function of pseudorapidity is shown in Figure 6. So there is considerable particle production in an LHC event that the detectors do not measure.

It is very common to present the positions of final-state particles of LHC events in momentum space using the variables (η, ϕ) (instead of (θ, ϕ). We can think of LHC events as being laid out on the (η, ϕ) plane, with typically 1 charged particle (and half a π^0) for each unit area on this plane.

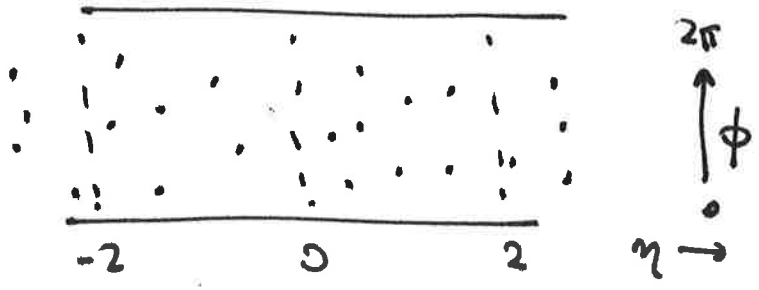

To discuss events with large momentum transfer, a very nice method is to plot the events in 3 dimensions, with each particle (or observed energy deposition) represented as a tower that its location in (η, ϕ) with height given by its p_T. This representation is called the "lego plot". Figures 7 and 9 show two events recorded by the DO detector at the Tevatron as tracks in the transverse section, and Figures 8 and 10 show the same events as lego plots. Note the very different scale of transverse momentum for the two events. The first event is a typical soft $p\overline{p}$ interaction. For the second event, the lego plot shows clearly that this event contains a $q\overline{q}$ hard scattering, resulting in two jets with approximately equal and opposite p_T.

More generally, the production of particles at large p_T requires some hard-scattering interaction. I estimate the rate of parton-parton hard scattering in lecture 2. We should now recall that figure, presented again as Figure 11. What is plotted is the integrated cross section down to the given value of p_T. As p_T ranges from 200 GeV to 2000 GeV, the rate decreases by 6 orders of magnitude. I also plot the event rate in events/sec, assuming a collider luminosity of $10^{33}/\text{cm}^2\text{sec}$. These rates are much lower than the total rate for pp inelastic scattering at this luminosity, 75 million/sec. Nevertheless, they are very substantial compared to the rate at which the LHC experiments can write data to permanent storage, about 200 events/sec. This means that it is necessary not only to ignore a large fraction of the soft events but also to reject a substantial fraction of hard-scattering events before any human has time to look at the data. The selection of the potentially most interesting events at a feasible data rate is done by the "trigger", a network of computers that rapidly analysis and route the incoming data. Any event that is preserved for analysis must have some special characteristics, with jets or leptons of sufficiently high p_T. This becomes an issue in particle searches, as I will discuss in lecture 7.

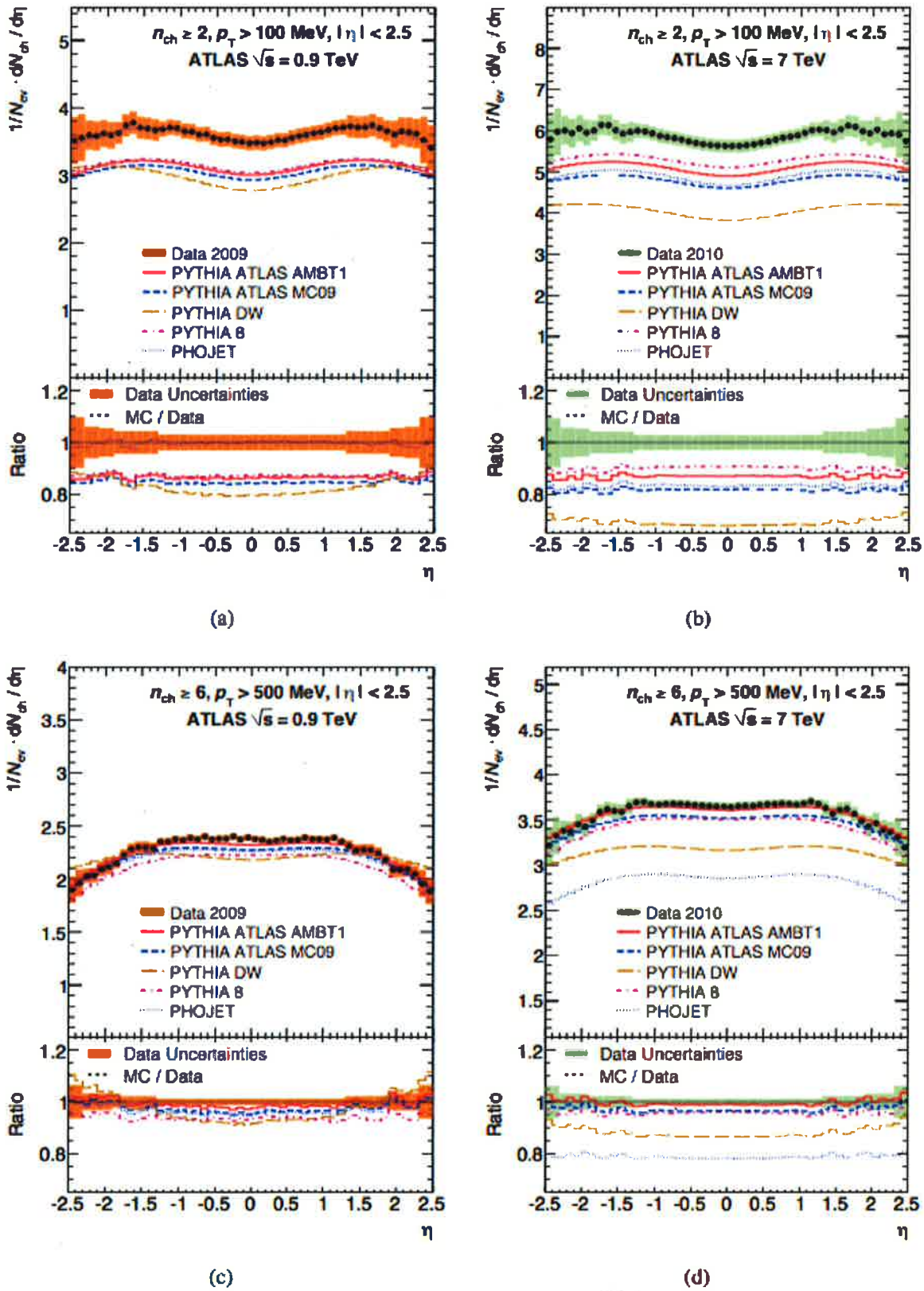

Fig. 6 Charged particle multiplicity $dN_{ch}/d\eta$ measured by the ATLAS experiment arXiv: 1012.5101, New J. Physics 13, 053033 (2011)

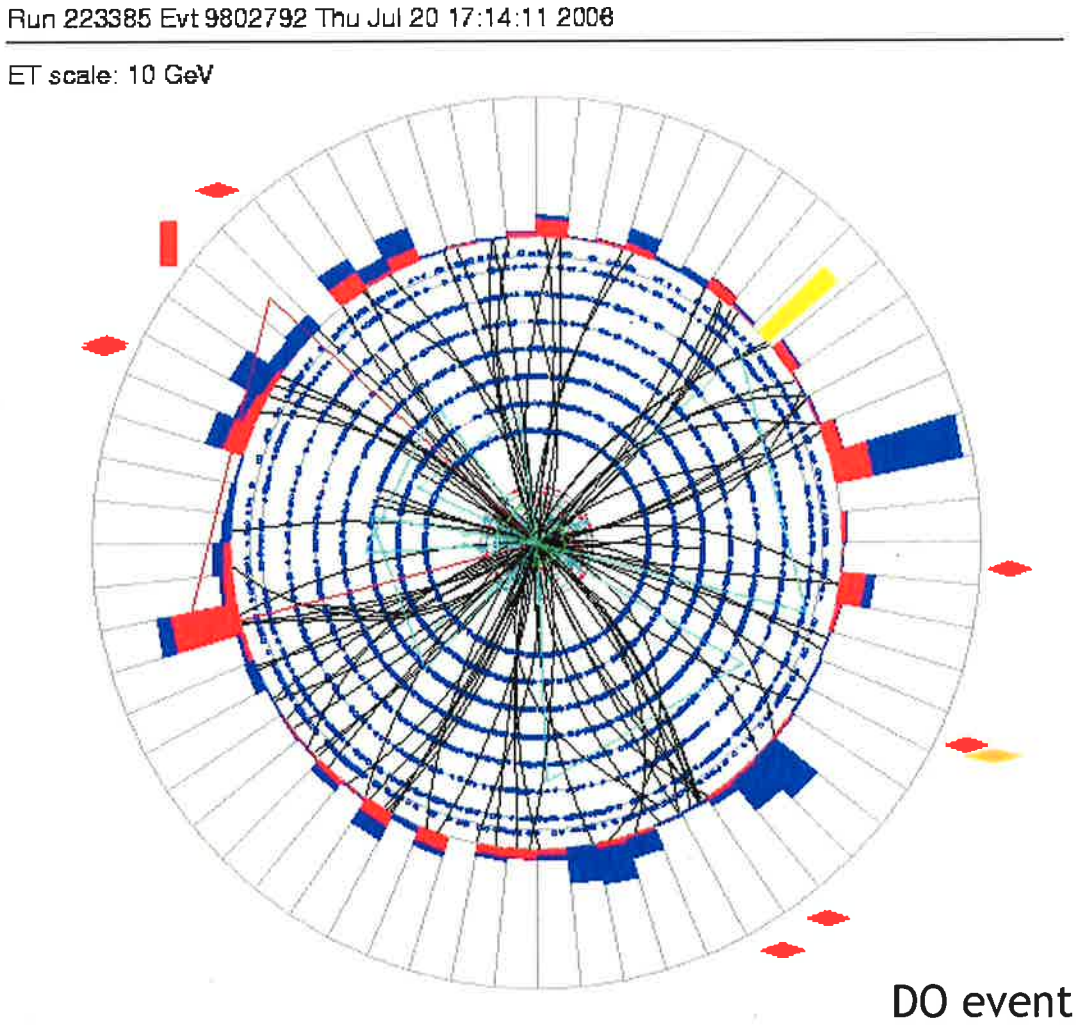

Fig. 7 Tracking view of an event from the DØ detector at the Tevatron.

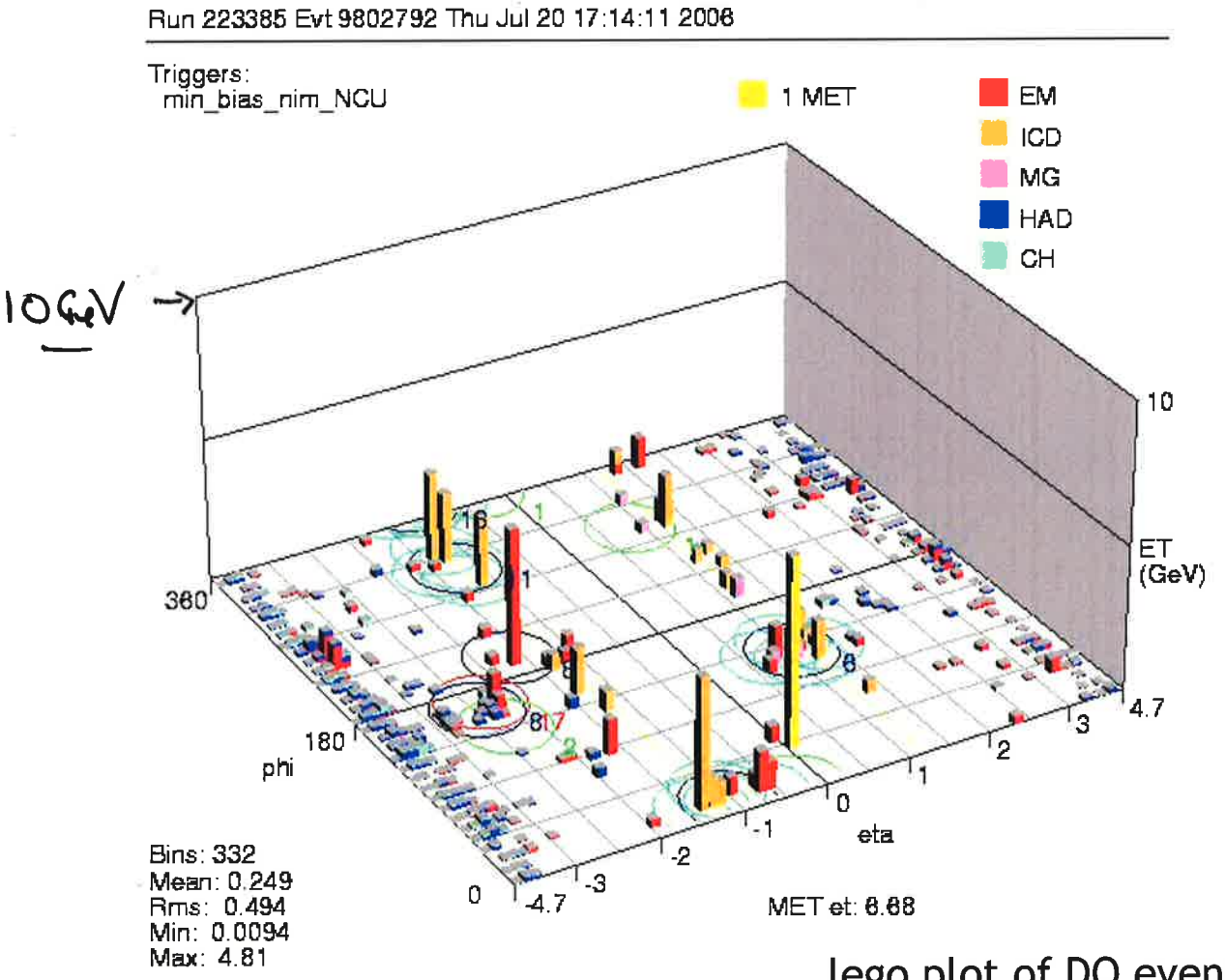

lego plot of DO event

Fig. 8 Lego plot of the same DØ event.

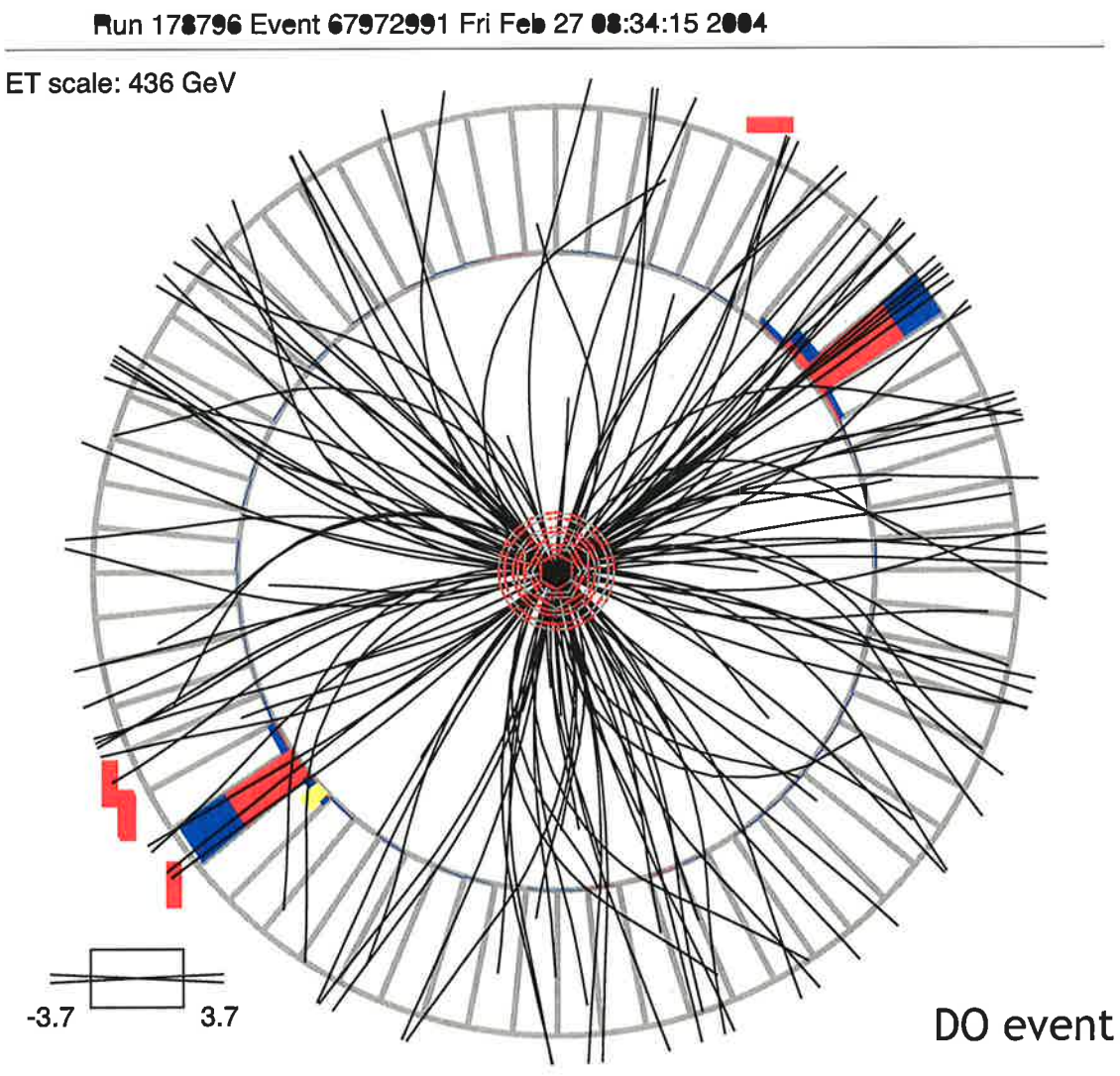

Fig. 9 Tracking view of a second event from the DØ detector at the Tevatron.

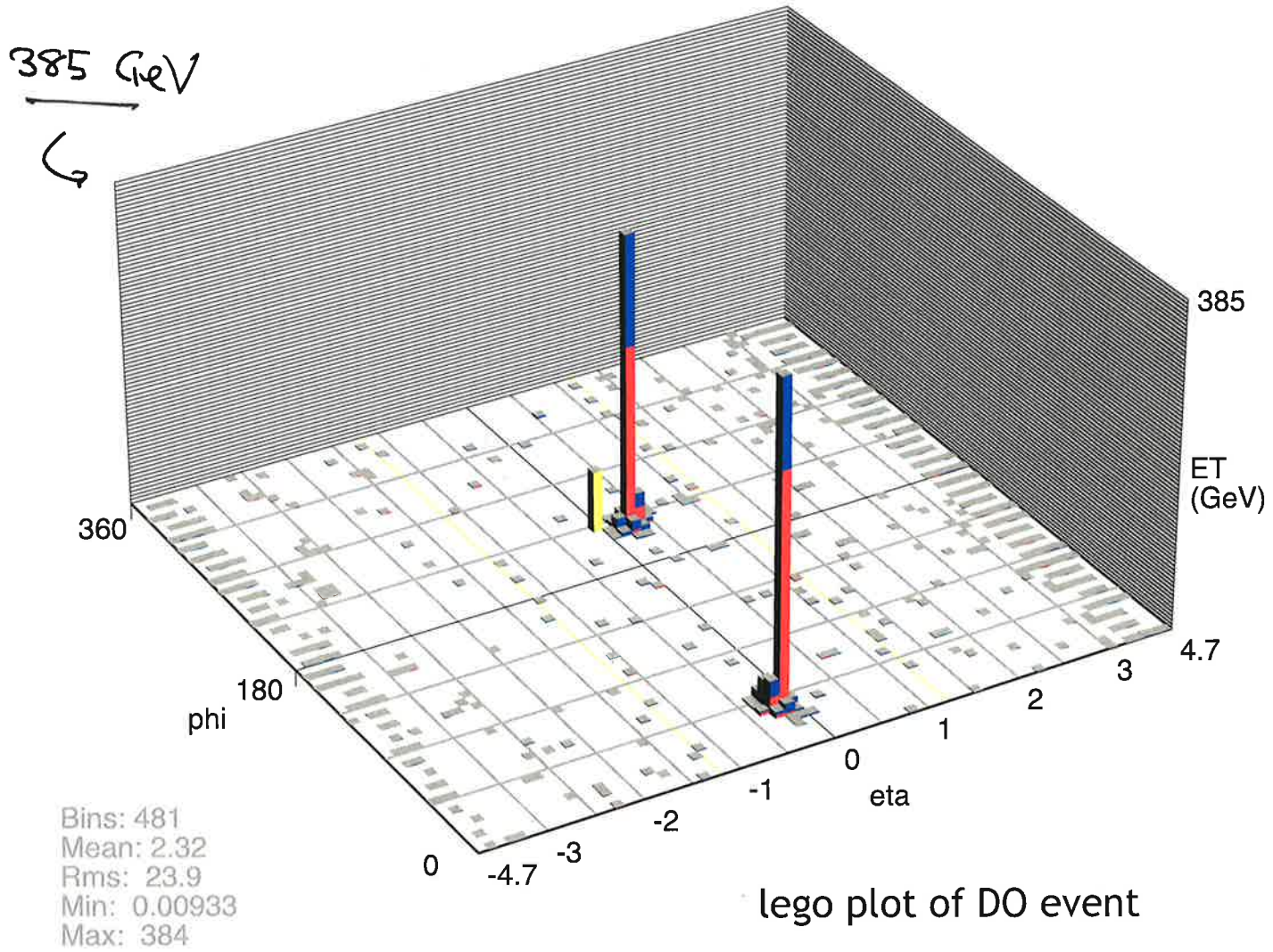

lego plot of DO event

Fig. 10 Lego plot of the same DØ event

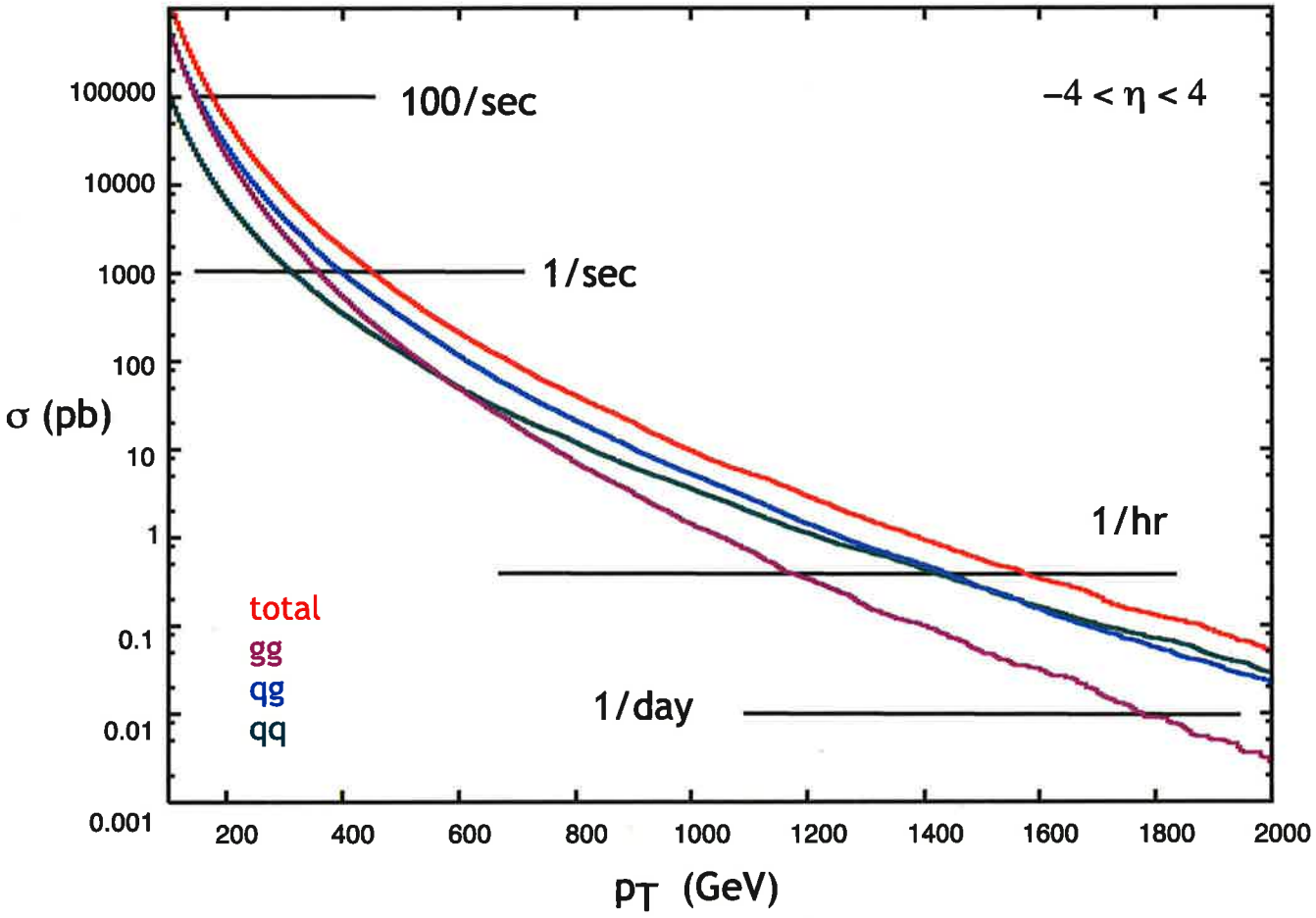

Fig. 11 Single parton-model estimate of the 2-jet cross section in pp collisions at 14 TeV. What is plotted is the integrated rate $\int_{p_T}^{\infty} dp_T \frac{d\sigma}{dp_T}$. Event rates are for a luminosity of $10^{33}/\text{cm}^2\text{sec}$.

Actually, the LHC already achieved a luminosity of $7.5 \times 10^{33}/\text{cm}^2\text{sec}$ in its previous run, and the expectation is that the luminosity will be several times higher in the coming run. So the problem of selecting events will be about an order of magnitude more difficult than the figure suggests.

The top of Figure 11 corresponds to a cross section of about 1μb for $p_T \sim 100$ GeV. The parton-parton cross section continues to rise for lower values of p_T, reaching 75 mb somewhere around $p_T \sim 20$ GeV. So, actually, every "typical" LHC event contains jet activity. The deviation of the curves shown in Figure 4 from a sharp exponential falloff is due to the presence of these jets. It is worth remembering that every LHC hard-scattering event also contains some additional jets not connected to the hard-scattering reaction.

Figure 12 and 13 show some parton-parton hard scattering events recorded by CMS and ATLAS. The track view shows only relatively high-p_T tracks; there are many more tracks with $p_T \sim$ 100-200 GeV. The very high p_T particles cluster into jets, which are apparent in the lego plots of the events.

Now we must discuss exactly what we mean by a jet. Even though jets are apparent in the event displays, it is not easy to give a precise definition of a jet suitable for quantitative analysis. In lecture 3, we described a jet as a cascade of almost collinear emissions from an initial high-momentum quark or gluon. The distribution of particles that results is approximately scale invariant, that is, fractal. It would be precisely scale-invariant if $\alpha_s(Q)$ were constant. In a fractal, any subcomponent of the object has the same structure as the original object. So we can choose to consider the particles produced by an ejected quark as comprising one jet or multiple jets, depending on the resolution with which we analyze the picture. This is a very important point: In QCD, jets are defined by convention, and different jet definitions lead to different quantitative predictions for the distribution and properties of jets.

Before discussing jets at the LHC, I will review properties of jets in e^+e^- collisions, as measured by the LEP experiments. In the e^+e^- environment, we do not need to worry about soft particle production in the "underlying event" or the production of particles invisibly at very forward rapidities. So it makes sense to look at all of the energy depositions seen by the detector and group these into clusters, which we will identify with the jets. This motivates the JADE algorithm for jet-finding: Start with a collection of observed particle momenta or energy depositions p_i. Define

$$y_{ij} = \frac{(p_i + p_j)^2}{s} = \frac{m^2_{(ij)}}{s}$$

Now proceed in steps, at each step combining the two momenta with the minimum

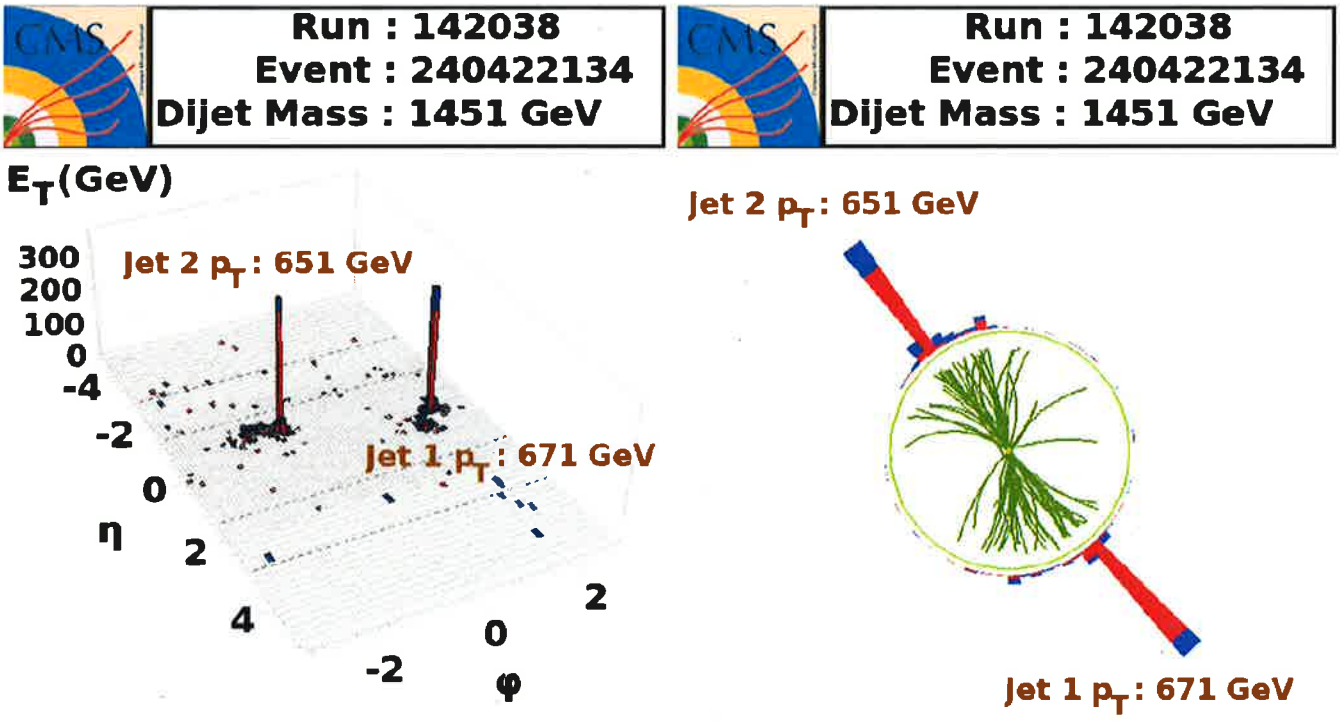

Fig. 12 A 2-jet event recorded by the CMS experiment at 7 TeV.

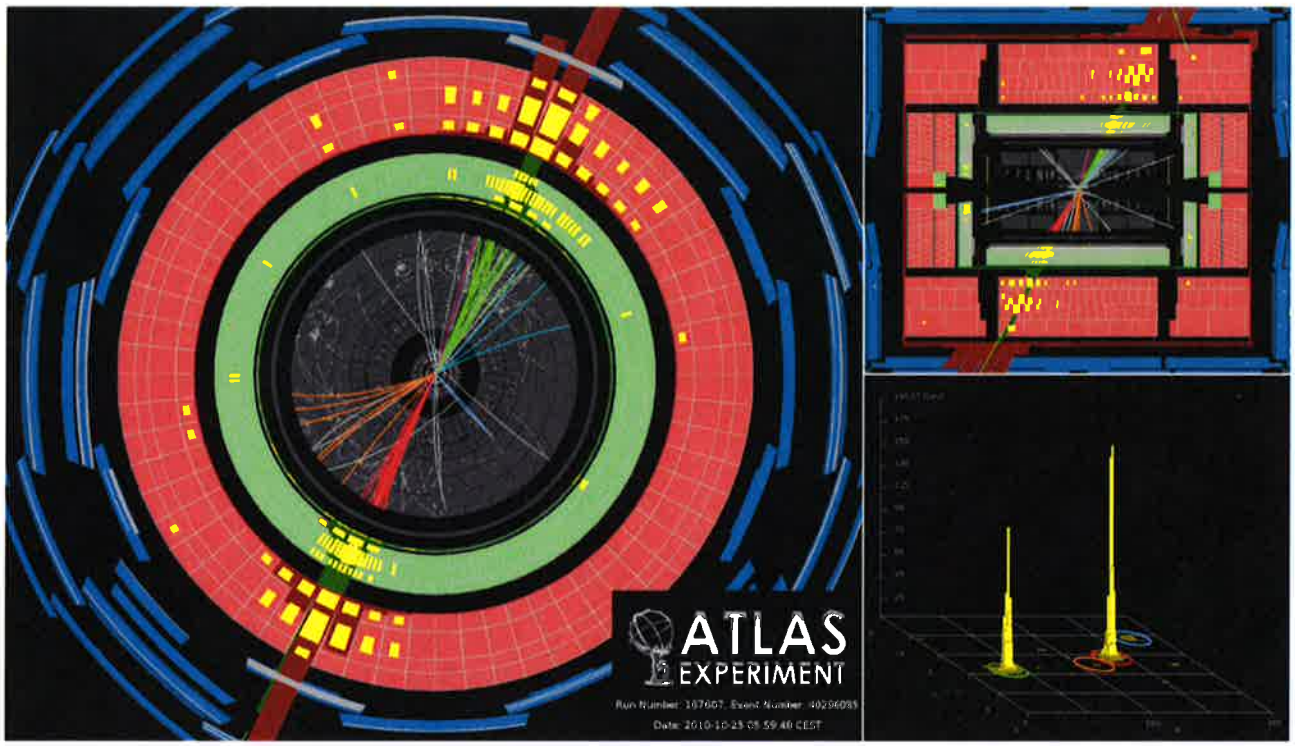

Fig. 13 2-jet event recorded by the ATLAS detector at 7 TeV. The jet p_T's are 1.2-1.3 TeV

value of y_{ij} into a single particle 4-vector. Continue until all particle pairs have y_{ij} greater than some specified value y_{cut}. The composite particles at this stage are defined to be the jets.

A typical setting for e^+e^- physics at Z energies is $y_{cut} = 0.01$, corresponding to a jet mass of 10 GeV. In the previous lecture, we saw that a parton splitting with transverse momentum p_T and energy fractions z, $(1-z)$ has an off-shell mass

$$m^2 = \frac{p_T^2}{z(1-z)}$$

Then, with this definition, a gluon emitted with $p_T > 5$ GeV generates a new jet. The ratio of 3-jet to 2-jet events can then be predicted by QCD. The ratio is proportional to $\alpha_s(y_{cut}s)$ and gives us a way to measure α_s.

The number of jets found in each event depends on the chosen value of y_{cut}. Figure 14 shows the fraction of events in e^+e^- annihilation at 206 GeV, measured by the ALEPH experiment at LEP, as a function of y_{cut}. These ratios can be predicted by QCD and, in fact, are compared to QCD calculations in the figure. The figure also makes clear the arbitrary nature of jets. For large y_{cut}, all events are 2-jet-like. For small values of y_{cut}, typically events are highly resolved into a large number of jets.

There are some requirements for a useful jet definition. In perturbative QCD, as we have seen, the probability for a collinear splitting is formally infinite, and also the probability to split off soft gluon is formally infinite. So, if we wish to have a reliable QCD computation of jet probabilities to compare with experimental results, the jet definition must be insensitive to these splitting processes. That is, the final jets found in an event should be the same whether or not these splittings occur. Such a jet definition is said to be "soft and collinear safe". The JADE algorithm satisfies this property. If we have a collection of partons and one radiates a soft gluon or undergoes a collinear splitting, the resulting 2-parton system has close to zero mass and therefore is recombined in the first step of the algorithm.

In hadron collisions, we do not measure the complete particle production. Thus, jet definitions must be local in the (η, ϕ) plane. At ATLAS and CMS, jets are defined mainly by electromagnetic and hadron calorimetry. To describe this most simply, the experiments associate an energy deposition and a value of p_T with each cell in a grid in (η, ϕ). Because the particle density within a jet can be large, a cell might contain more than one particle. Now we have a set of calorimeter objects

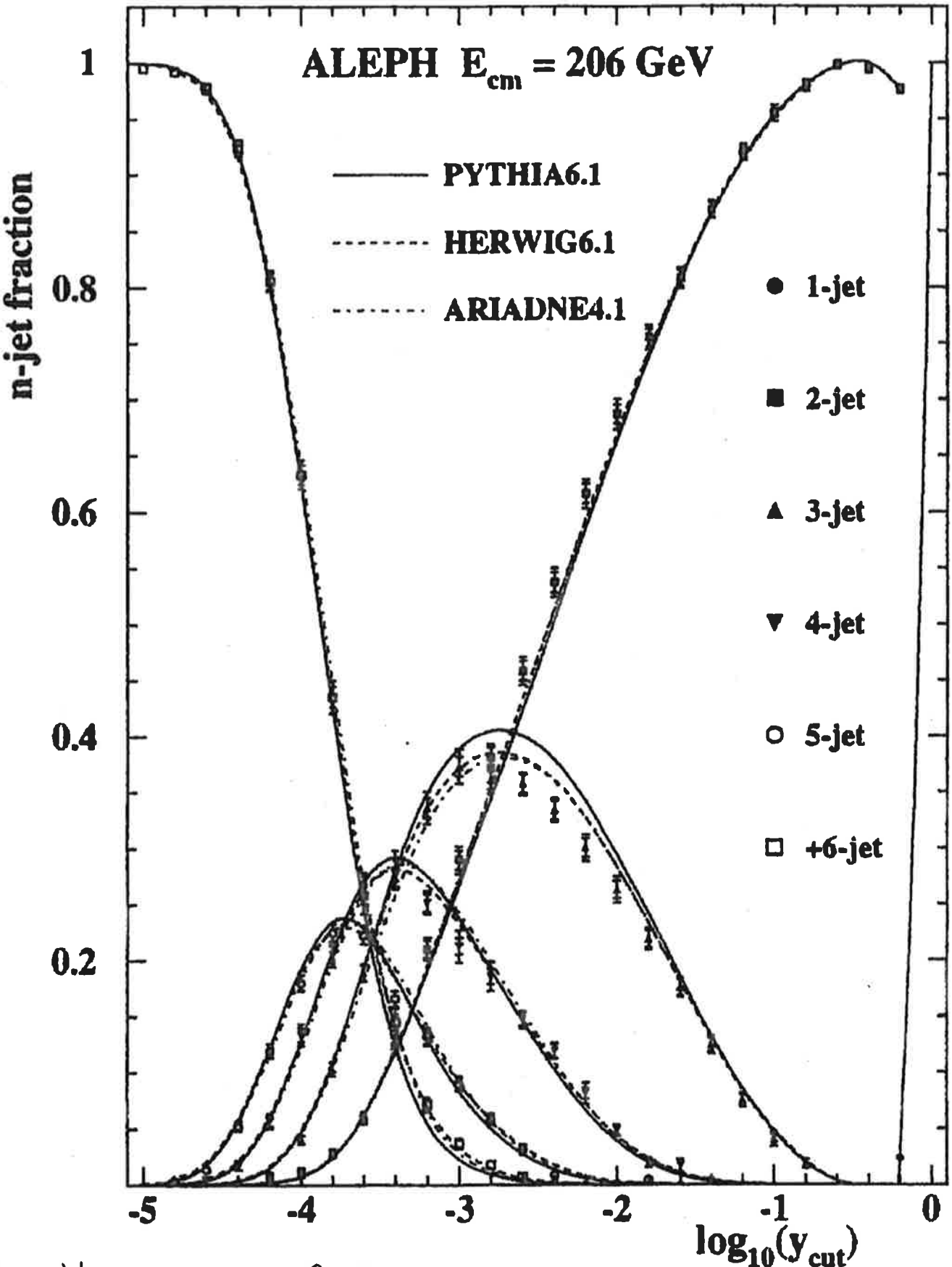

Fig. 14 Fractions of $e^+e^- \to$ hadrons events at 206 GeV containing n jets. From A. Heister et al Eur. Phys. J C 35 457 (2007).

$$\{\eta_i \ \phi_i \ p_{Ti}\}$$

Define a distance between these objects as follows: Let

$$\Delta R_{ij} = \left[(\eta_i - \eta_j)^2 + (\phi_i - \phi_j)^2\right]^{\frac{1}{2}}$$

be the separation in the (η, ϕ) plane. Let the distance between objects i and j be

$$d_{ij} = \min\left(p_{Ti}^{2\alpha}, p_{Tj}^{2\alpha}\right) \cdot \frac{\Delta R_{ij}^2}{R^2}$$

and let the distances from the object i and the beam be

$$d_{iB} = p_{Ti}^{2\alpha}$$

A jet algorithm will combine these objects, beginning with the pair with the smallest value of d. An object will drop out of consideration when the minimum distance is between that object and the beam. When the process is complete, the objects associate with the beam are defined to be the jets.

For clarity, consider $\alpha = 0$. Then, roughly, the objects that are closer than a distance R will be combined. There is some subtlety in this process, since the positions of objects shift as they are combined. However, the procedure is very close to the idea of drawing circles of radius R on the (η, ϕ) plane and moving those circles around until they include the largest possible amount of the total transverse momentum. This latter algorithm (which needs additional steps if the circles overlap) is called the "cone jet algorithm".

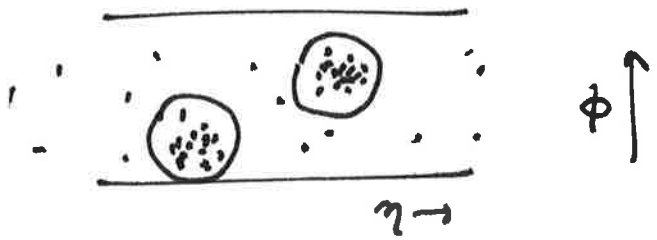

The distance algorithm with $\alpha = 0$ is called the "Cambridge/Aachen algorithm". To have the jet combination process more closely mimic the JADE algorithm, we can set $\alpha = 1$. This is called the "k_T algorithm". With this algorithm, objects with small p_T are more easily associated—but not necessarily with the closest jets. Cacciari, Salam, and Soyez noticed that the distance algorithm is actually infrared and collinear safe for all values of α, including negative values. They suggested using the "anti-k_T algorithm", with $\alpha = -1$. This algorithm causes an object with large p_T to soak up all of the neighboring objects with small p_T, leading to smooth, round clusters in the (η, ϕ) plane. A comparison of the jets found in the same event with this different algorithms is shown in Figure 15.

The anti-k_T algorithm is the standard one used for most analysis by both ATLAS and CMS, though other algorithms are also useful for specific purposes. There is also the question of choosing the best value of R. In principle, this should balance two effects, the decrease in the jet p_T due to radiation out of the cone and the increase in the jet p_T due to absorption of soft hadrons from the underlying event. ATLAS and CMS make different choices, using as a standard $R = 0.4$ and $R = 0.5$, respectively.

A splitting with large p_T can always produce QCD radiation outside the cone, so QCD will naturally generate events with additional jets. The approximately scale-invariant nature of QCD tells us that we should find events with any number of jets, with a smoothly decreasing probability. Figure 16 shows the inclusive cross sections for n jet production measured by ATLAS, up to $n = 6$. The probability of an additional jet is about 10%, comparable to

$$3\,\frac{\alpha_s}{\pi}$$

(This number depends on the minimum p_T in the sample of jets.) The pattern seen here, with the rate for additional jets steadily decreasing on a log scale, is called a "staircase"; it is a commonly seen feature in LHC physics. Figure 17 shows a 6-jet event recorded by the ATLAS experiment.

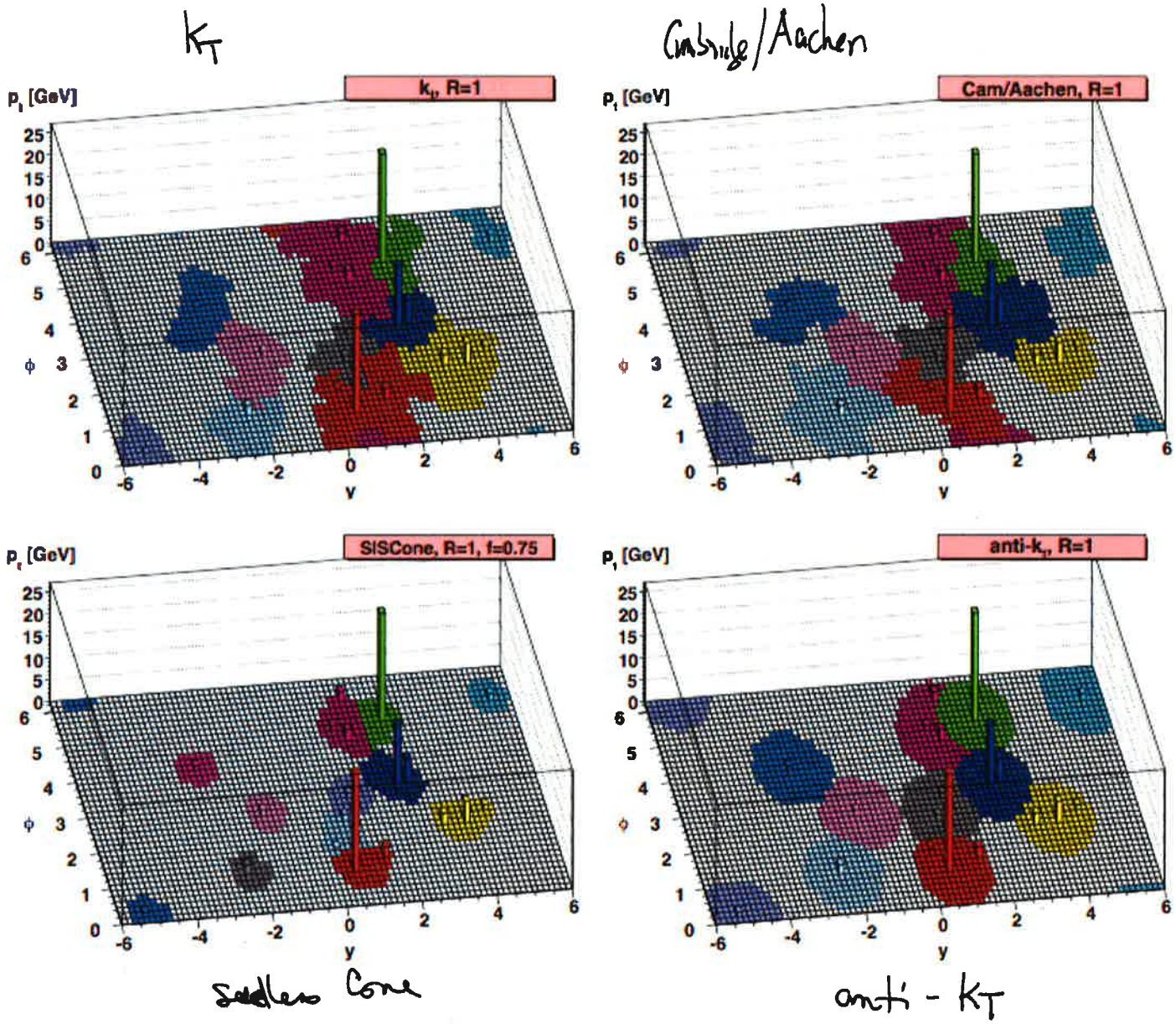

Fig. 15 Jets found in the same (simulated) LHC event by four different jet algorithms, from G. Salam arXiv: 0906.1833, Eur. Phys. J C67 637 (2010).

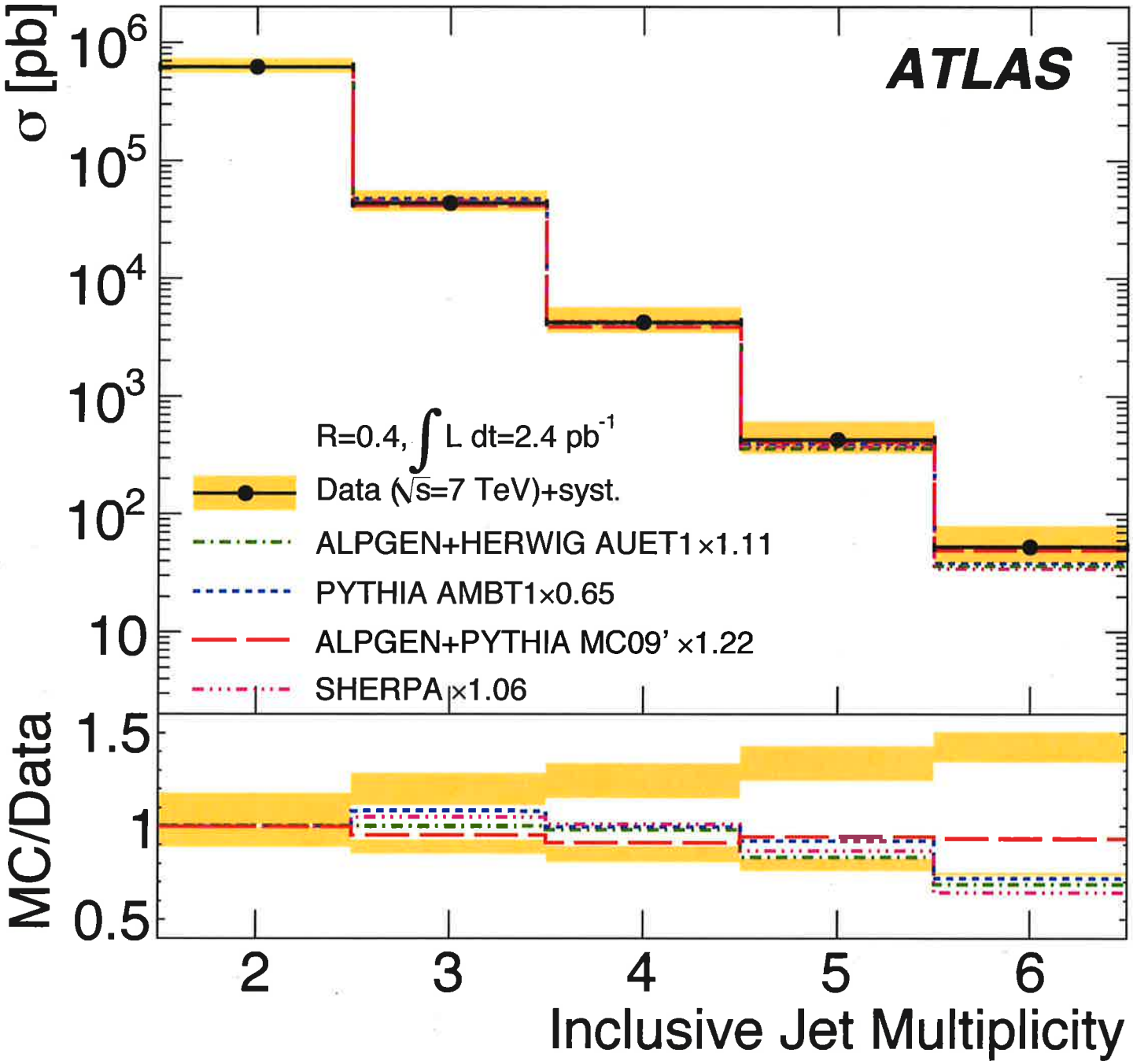

Fig. 16 Inclusive cross sections for ≥ n jets at 7 TeV, measured by the ATLAS experiment, arXiv: 1107.2092 (Eur. Phys. J C71, 1763 (2011)).

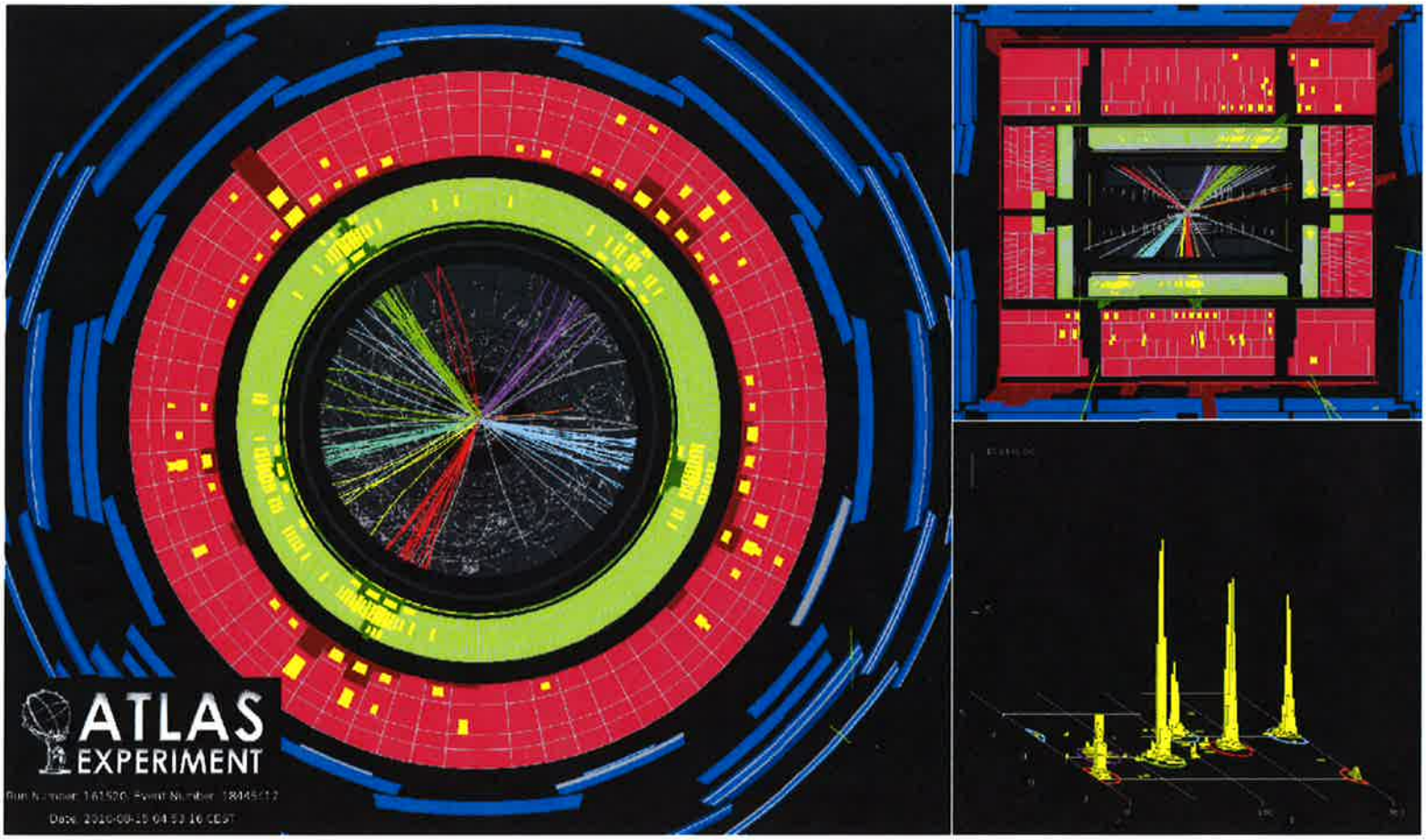

Fig. 17 6-jet event recorded by the ATLAS detector at 7 TeV.

The overwhelming rate and potential great complexity of QCD events make it difficult to use these events to discover new physics processes at the LHC. For this reason, most searches for new physics rely on properties of the final state that are not expected in QCD. These include the presence of leptons and of "missing energy", that is, unbalanced momentum, in the event.

The term "missing energy" deserves some comment. I have already pointed out that the ATLAS and CMS experiments measure particle production only in the central rapidity region. So, using these detectors, it is not possible to determine whether the longitudinal momentum in an event is unbalanced. However, it is possible to observe an imbalance of transverse momentum. The term "transverse energy" or E_T is used to represent the scalar sum of the observed energy depositions of particles, each projected onto the dimensions transverse to the beam direction. Similarly, "missing transverse energy", $\not\!\!E_T$ is the vector sum of the measured transverse energies of particles. It must be emphasized that $\not\!\!E_T$ is very tricky to measure, since it can be generated if parts of the detector are not working correctly, or by fluctuations in the measurement of jet energy in multijet events. The LHC experiments have done a remarkable job of controlling or compensating for these effects. The resolution in $\not\!\!E_T$ for ATLAS is shown in Figure 18. Note that this goes as $\sqrt{E_T}$ as one might expect for a quantity generated by fluctuations.

It is important, then, to understand the Standard model processes at the LHC that generate leptons and $\not\!\!E_T$, especially in combination with jets. These include reactions that produce one or more W or Z bosons and reactions that produce top quarks and antiquarks.

Figure 19 gives the QCD predictions for cross sections for the whole range of reactions found at the LHC. The units are nb. The Drell-Yan cross sections for the production of W and Z are at the hundred nb level. These must of course be multiplied by the branching ratios computed in lecture 1 to find the rates of producing leptonic or $\not\!\!E_T$ final states. The top quark pair production cross section is at the hundred pb level, rising to close to 1 nb at 14 TeV. The single top process, discussed below, has a comparable rate. Processes with production of pairs of vector bosons, with electroweak cross sections, are also at the 100 pb level. We can add radiated jets to any of the events, at cost of about 0.1 per jet in rate. All of these processes provide backgrounds to searches for new particles, as we will discuss in lectures 6 and 7.

Notice that the presence of b quarks, alone, is not useful as a signature of unusual physics in an LHC event. The QCD cross section to produce a pair of b quarks is close to 1 mb at 14 TeV. (It is true that many of these quarks are emitted into the forward rapidity region.) However, many of the objects of LHC searches specifically involve b quarks and can be searched for using b vertex tagging in conjunction with other signatures.

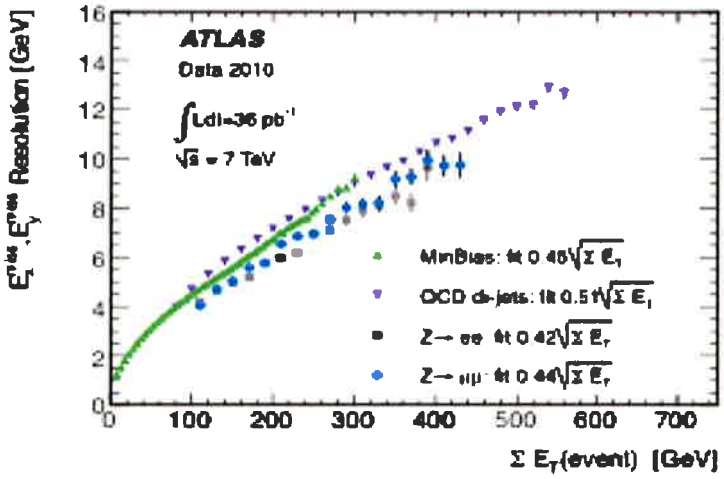

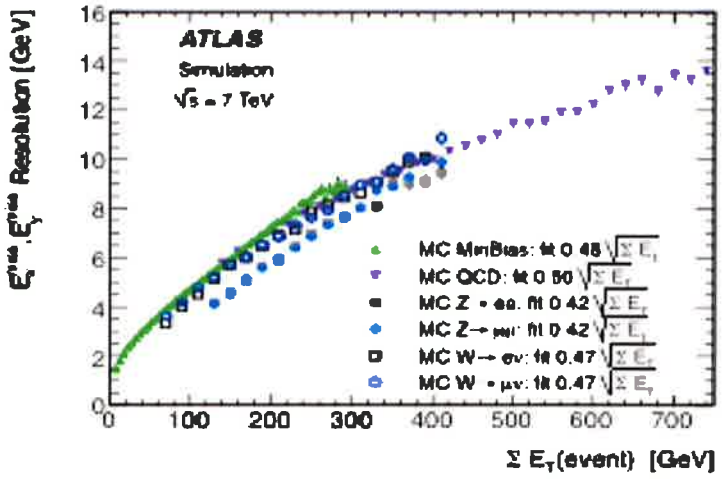

Fig. 18 Resolution in $\not{E}_T$ measured for the ATLAS detector, plotted as a function of the total transverse energy, from arXiv: 1108.5602, Eur. Phys. J. C72 1844 (2012).

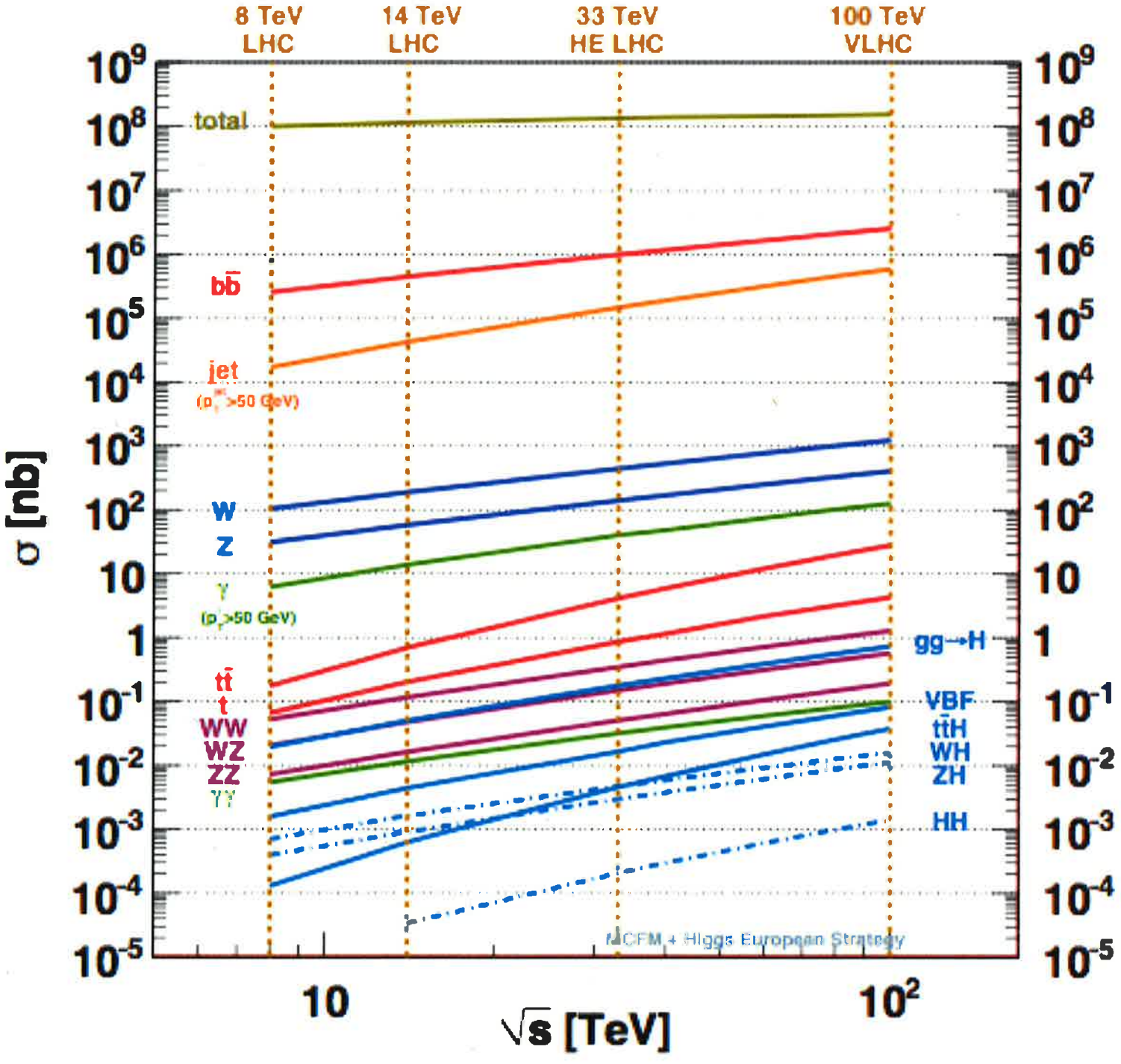

Fig. 19 QCD prediction for cross sections of a variety of processes at pp colliders, from J M Campbell et al. arXiv: 1310.5189.

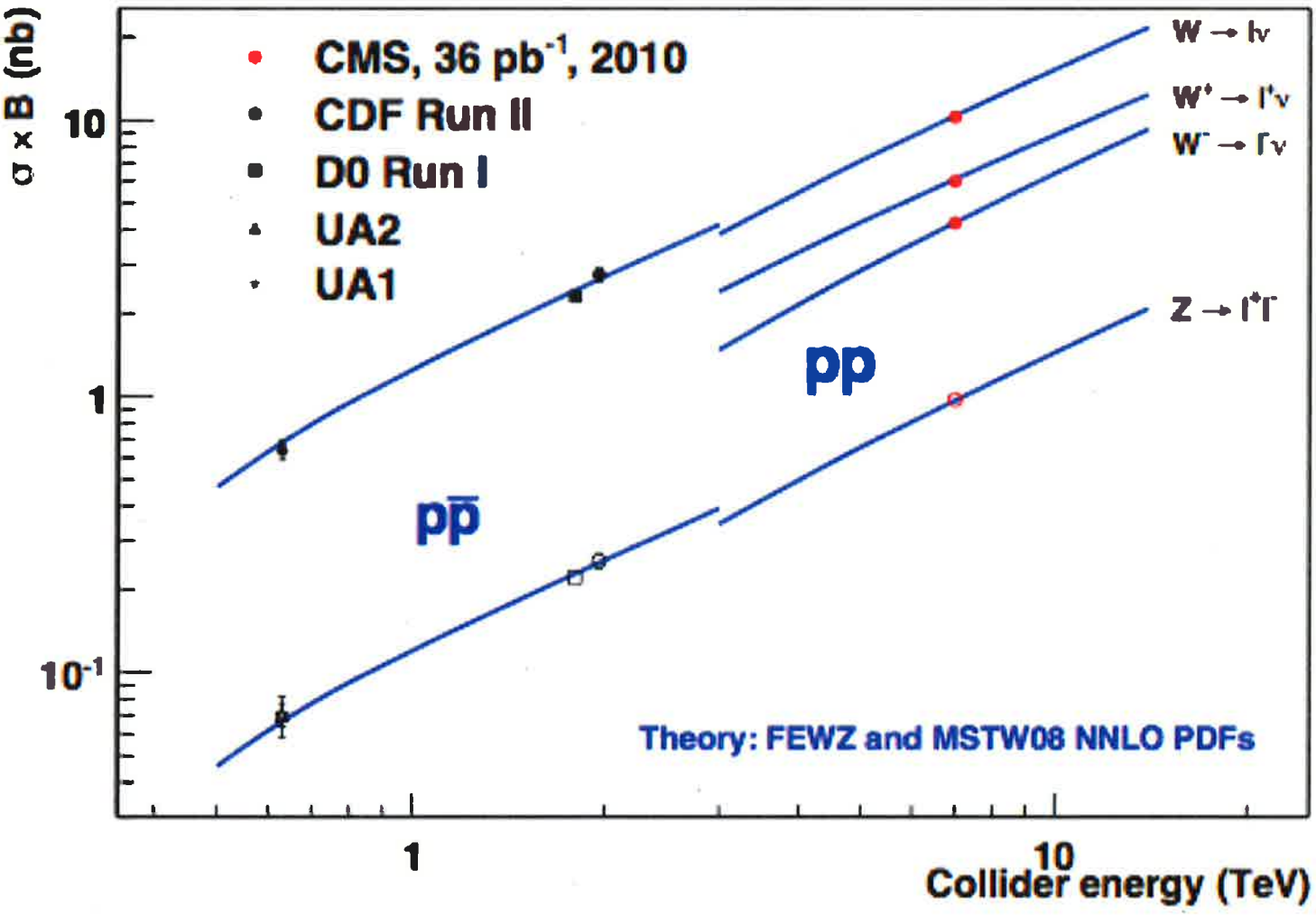

Fig. 20 The cross sections for $p\bar{p} \to W \to l\nu$ and $Z \to l^+l^-$ measured at the LHC and at lower energies, from CMS Collaboration arXiv: 1107.4789, JHEP 1110, 132 (2011)

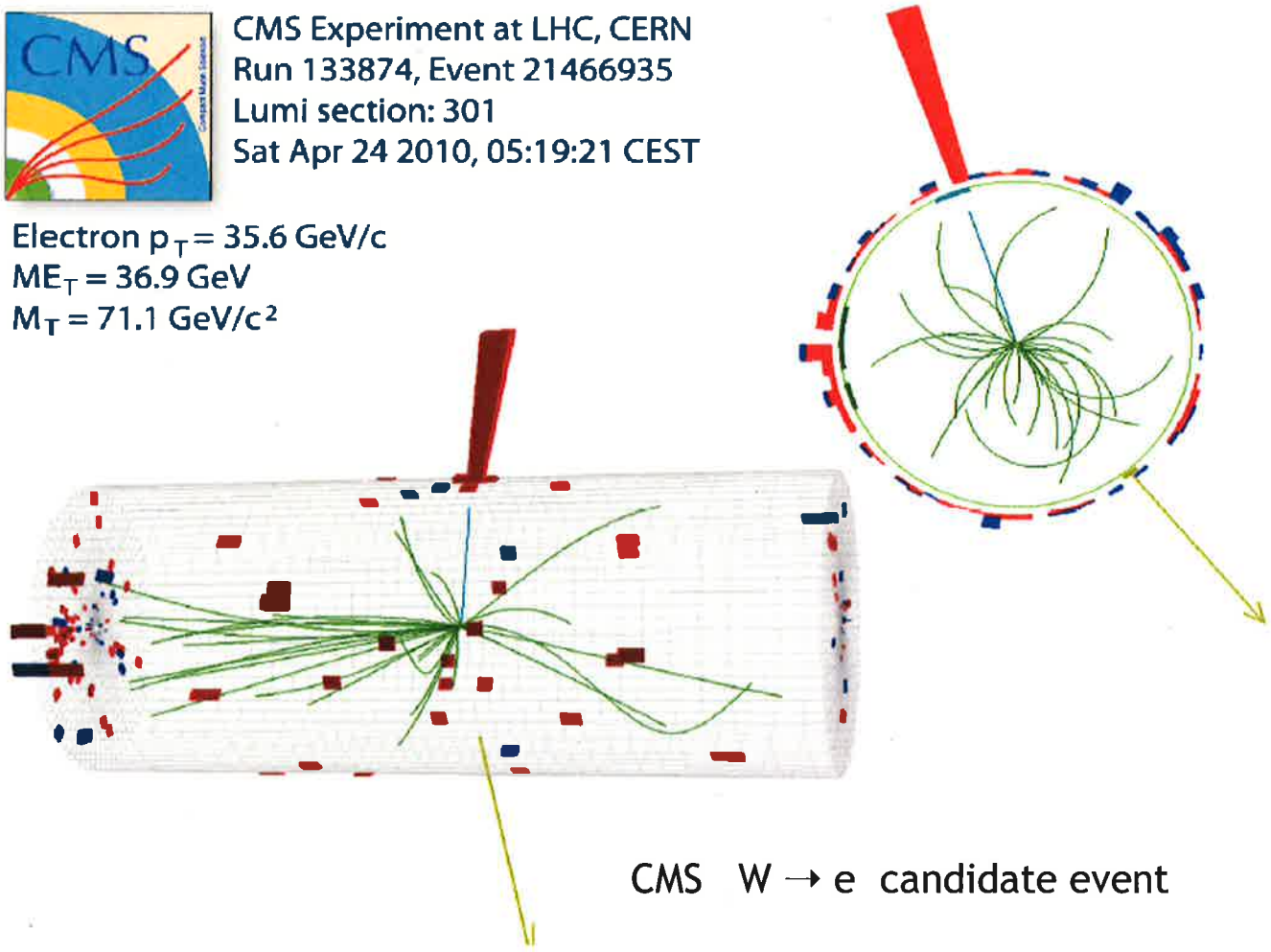

Fig. 21 A candidate $pp \to W \to e\nu$ event recorded by the CMS experiment at 7 TeV.

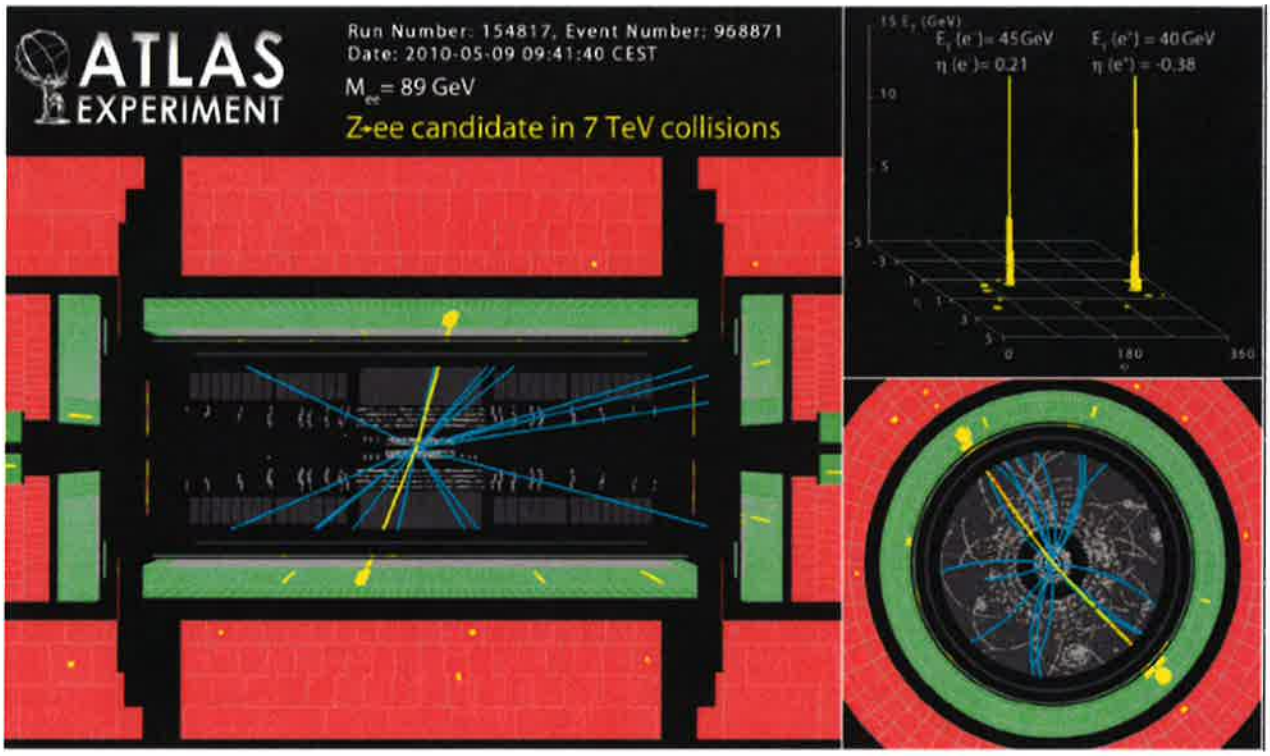

Fig. 22 A candidate $Z^0 \to e^+e^-$ event recorded by the ATLAS experiment at 7 TeV.

I would now like to discuss each of these processes in somewhat more detail. We computed the parton model prediction for the Drell-Yan cross sections in lecture 2 and discussed some of their qualitative features there. The QCD prediction for the Drell-Yan cross sections are now known to NNLO, that is, to few-percent accuracy. These predictions are in excellent agreement with the measured cross sections, as shown in Figure 20. The cross sections shown here include the leptonic branching ratios. Recall that the branching ratio of the Z to $\ell^+\ell^-$, $\ell = e, \mu$, is quite small, only 5%. The cross section for producing $Z \to \nu\overline{\nu}$, which is a Standard Model source of $\not{E}_T$, is 4 times larger. Figure 21 shows an event display fromr a candidate $W \to e\nu$ event from CMS. Figure 22 shows an event display from a candidate $Z \to e^+e^-$ event from ATLAS.

It is interesting to select for events that contain $\ell + \not{E}_T$ or $\ell^+\ell^-$ plus jets. Figure 23 shows the inclusive cross sections measured by ATLAS for events consistent with $W \to \mu\nu$ with n jets. Again, we see a staircase down to very high numbers of jets. The vertical axis is a log scale, so for small jet numbers these events are dominated by Drell-Yan production with extra partons radiated from the intial state quark and antiquark. However, the model shown that fits the data indicates that for large numbers of jets, the dominant production mechanism is $pp \to t\bar{t}$. Note also the large contribution of $Z \to \mu * + \mu^-$ events in while one muon is not observed, typically because it is produced into the high-rapidity region. The implication of this plot, that LHC data sets are typically composed of a wide variety of processes, all of which must be modelled, is a common principle in interpreting LHC data. The similar plot for Z is shown in Figure 24. It is remarkable that even the clean $Z \to \mu^+\mu^-$ signature can be faked by other processes.

The top quark is the one quark heavy enough to decay to an on-shell W boson. Only the CKM element V_{tb} is large, so top quark decays are mainly $t \to Wb$, with the W then decaying to leptons and quarks according to the branching ratios computed in lecture 1. There are then three distinct classes of top quark pair production events, those with leptonic decays of both the top and antitop, one leptonic and one hadronic decay (also called "semileptonic"), and those with hadronic decays on both sides. The cross section for top quark pair production can be measured in all three modes. A composite of the LHC measurements, together with the pair production cross section for $p\overline{p} \to t\bar{t}$ measured at the Tevatron, is shown in Figure 25. It is remarkable that the cross section at the LHC is larger that that at the Tevatron by a factor of 30, even with the replacement of $p\overline{p}$ with pp initial states. The explanation for this is twofold. Top quark pairs can be produced both from $q\overline{q}$ annihilation and from gg annihilation, through the diagrams

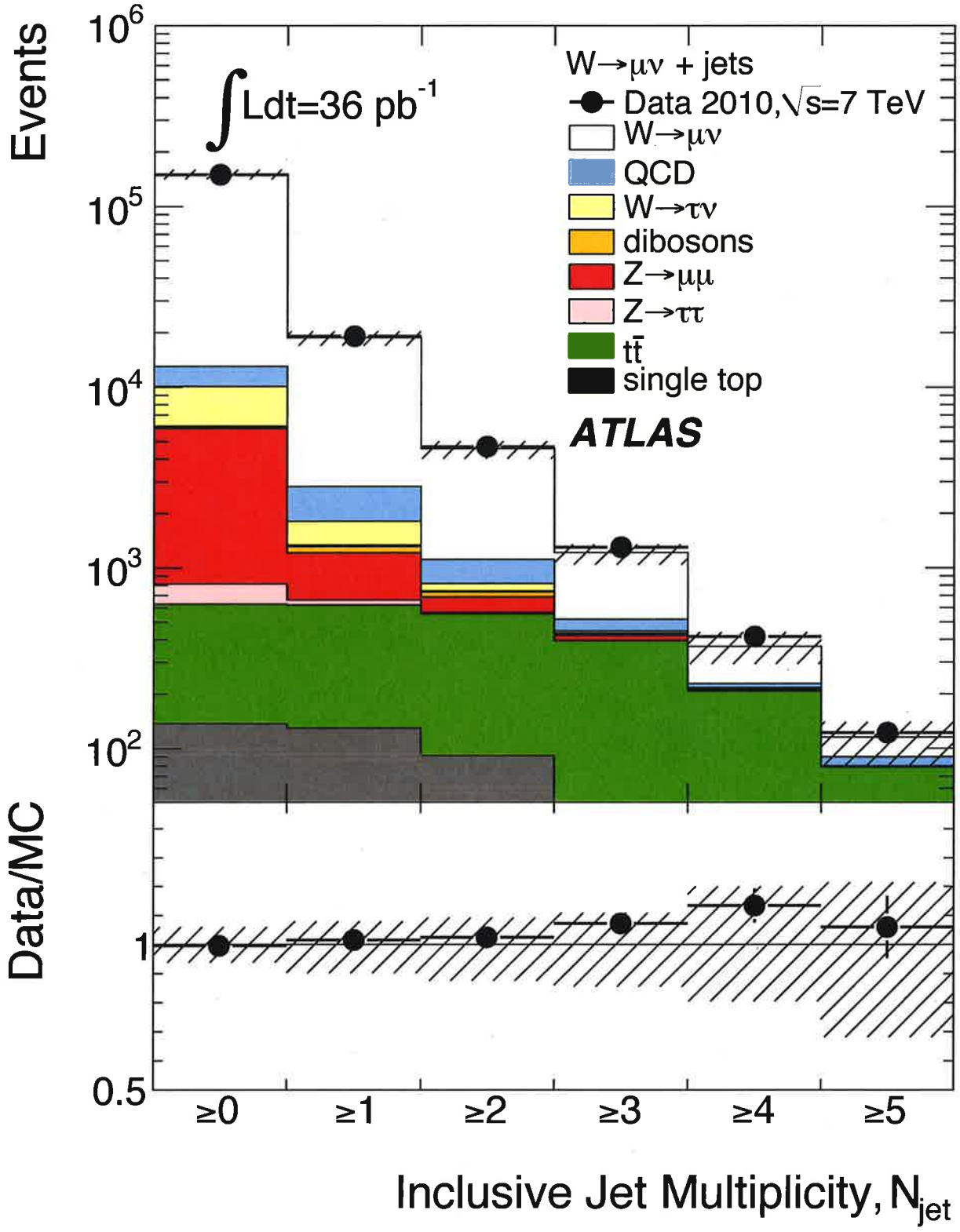

Fig. 23 Inclusive cross section for events with ≥ n jets measured by the ATLAS experiment for events consistent with W→μν. arXiv:1201.1276 Phys Rev D 85, 092002 (2012)

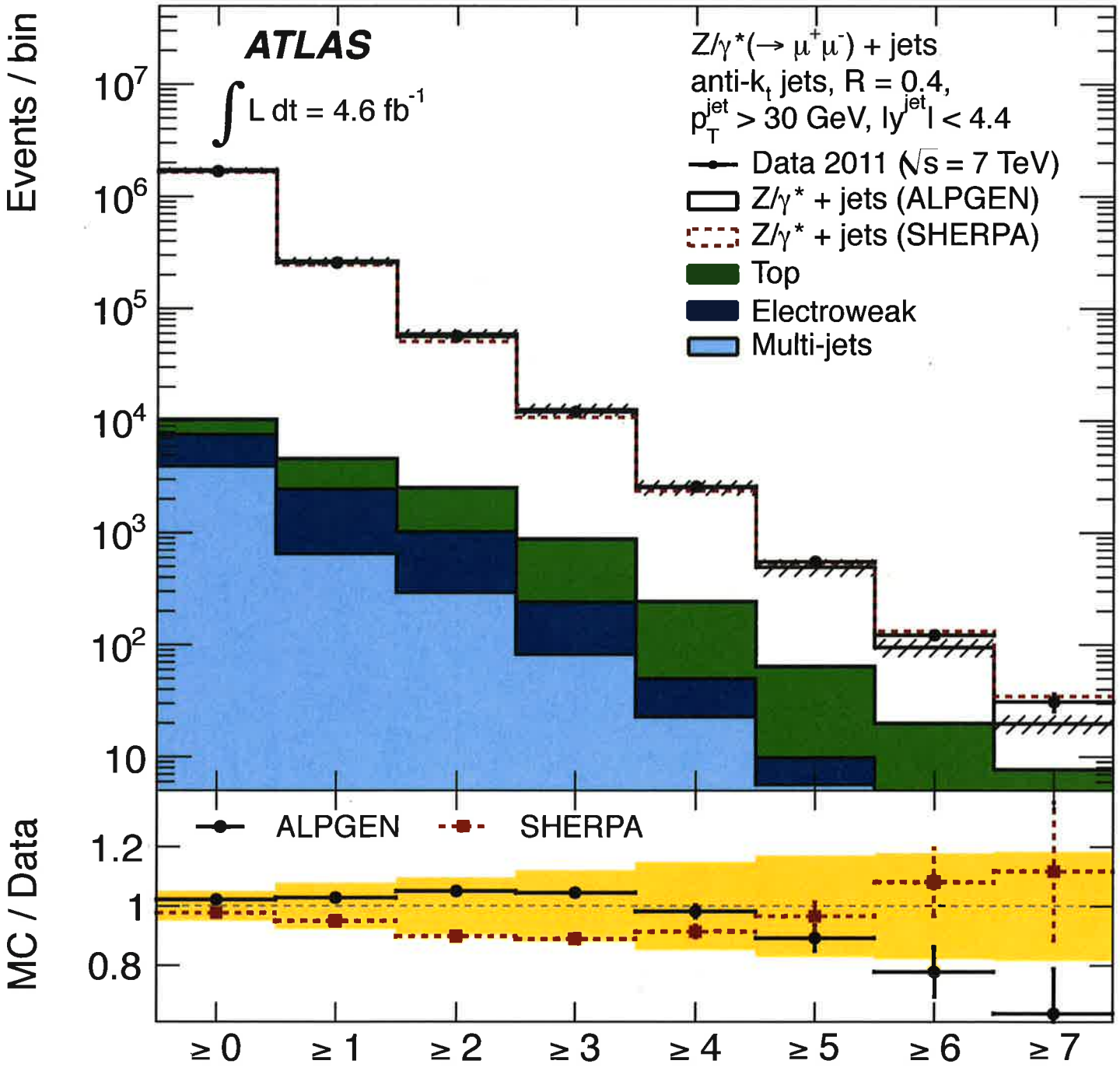

Fig. 24 Inclusive cross sections for events with $\geq n$ jets, measured by the ATLAS experiment at 7 TeV for events consistent with $Z \to \mu^+\mu^-$, arXiv: 1304.7098 (JHEP 07 (2013), 032).

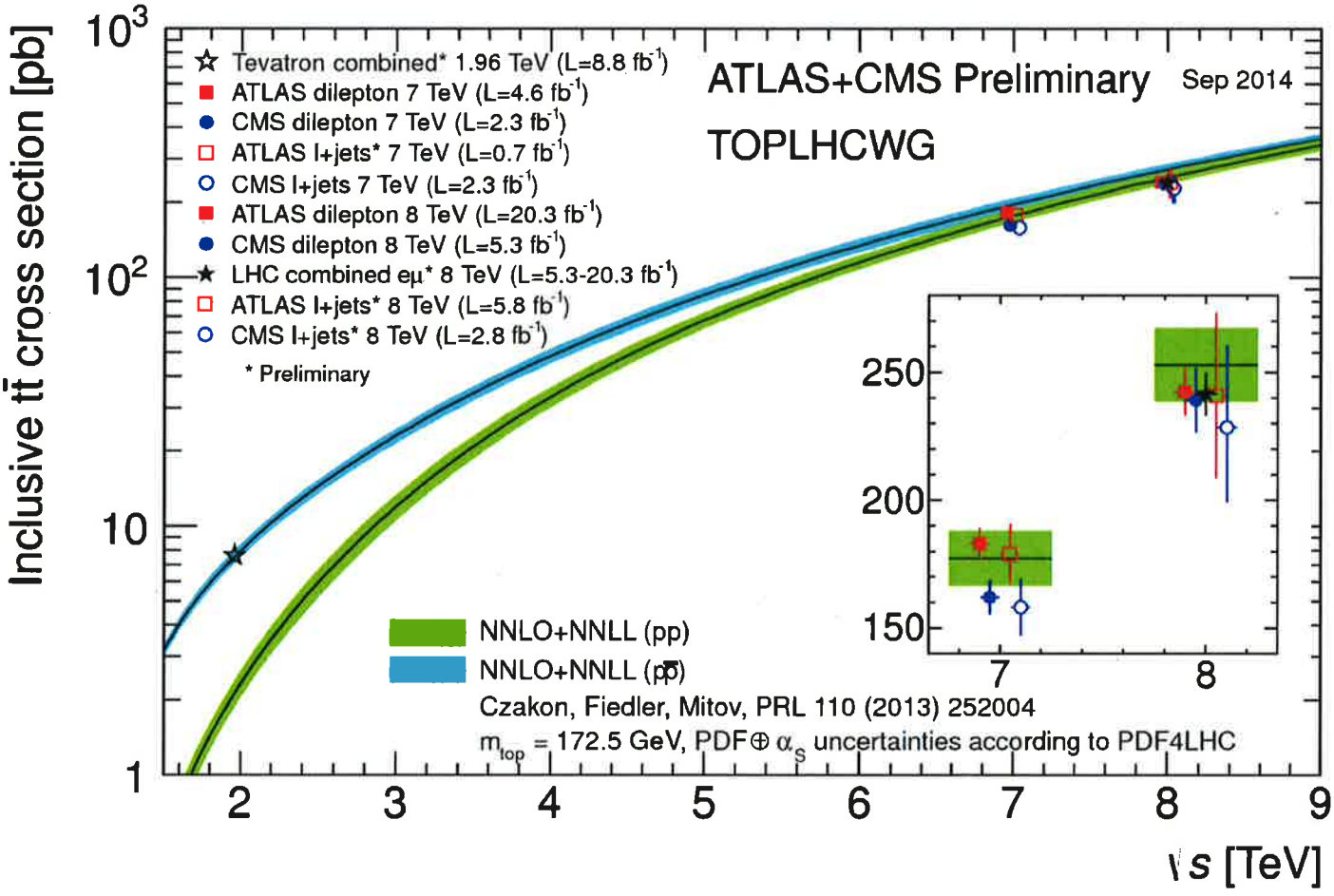

Fig. 25 Cross sections for $p\bar{p} \to t\bar{t}$ and $pp \to t\bar{t}$ measured at the Tevatron and the LHC, from the Top LHC Working Group combination. See ATLAS-CONF-2014-054.

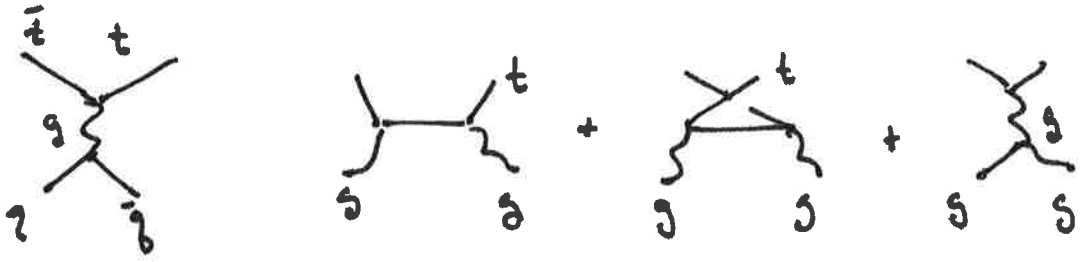

The gluon diagrams are numerically larger about a factor of 10, due to color factors and t-channel exchange. At the Tevatron, the gluons are typically not energetic enough to make t quark pairs. At the LHC, we can take advantage both of the numerical factors in the gg cross section and of the dramatic rise of the gluon pdfs at small x. The figures shows the comparison of the LHC data with the new NNLO cross section calculation by Czakon, Fiedler, and Mitov. The agreement of theory and experiment is excellent.

Figure 26 shows an ATLAS event display with an excellent candidate for $t\bar{t}$ production. A semileptonic $t\bar{t}$ event contains in the final state

This event indeed contains an electron, $\not{E}_T$, and 4 jets, including one b-tagged jet.

The cross section for $t\bar{t}$ pair production is very large compared to cross sections for LHC events of similar complexity. This is excellent for studying the top quark, since relatively simple event selections produce samples dominated by $t\bar{t}$ production. For example, Figure 27 shows the 3-jet mass distribution from a CMS analysis that demands 6 jets, with 2 b-tagged, and 2-jet pairs consistent with the W mass in the expected final state

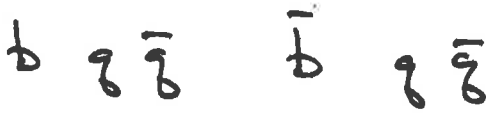

The peak at the top quark mass of about 170 GeV is apparent. The large size of the top quark pair production cross section, however, makes this an important background when searching for other types of processes at the LHC, as we have already seen in Figures 23 and 24.

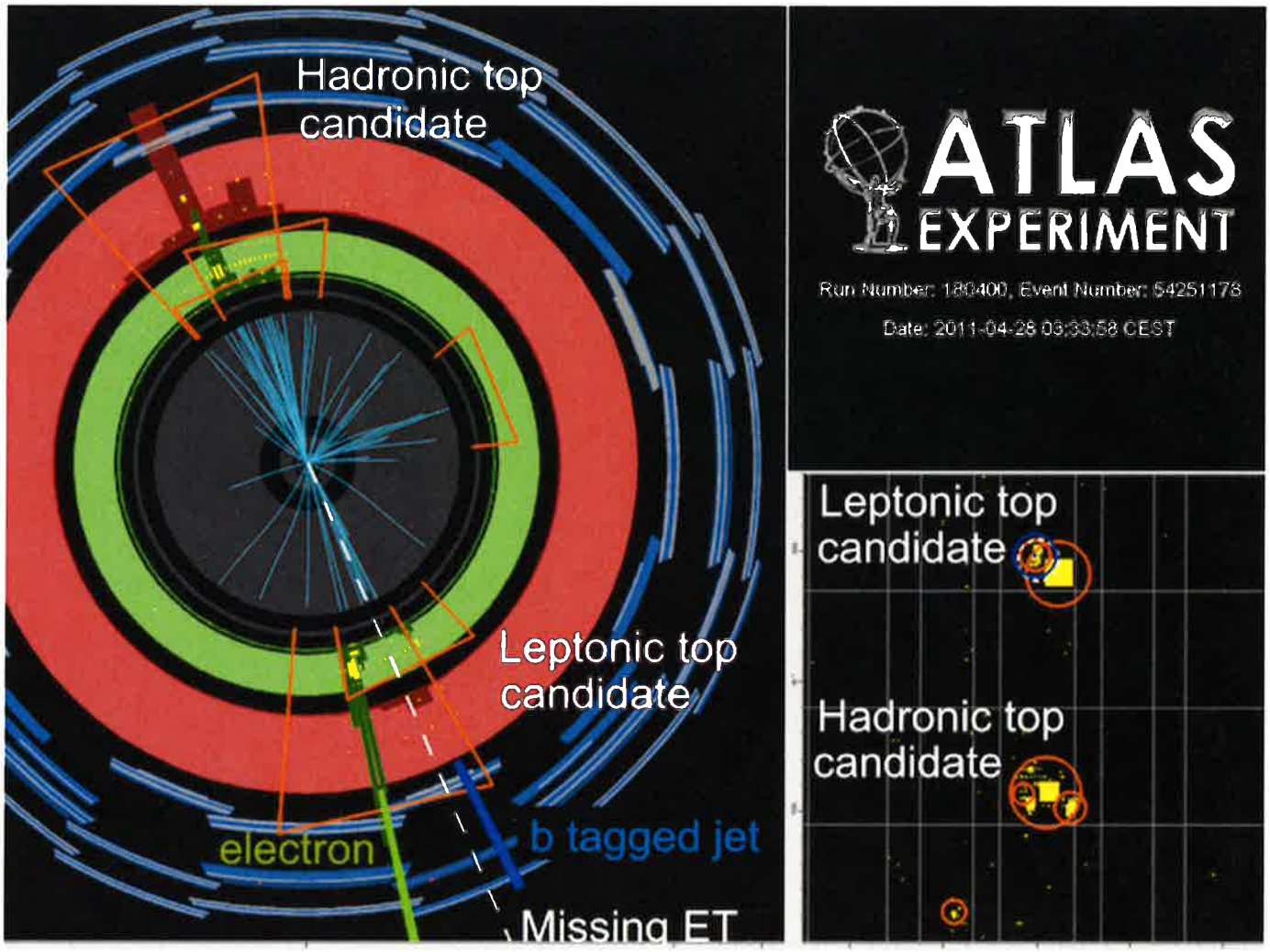

Fig. 26 A candidate $pp \to t\bar{t}$ event recorded by the ATLAS experiment at 7 TeV.

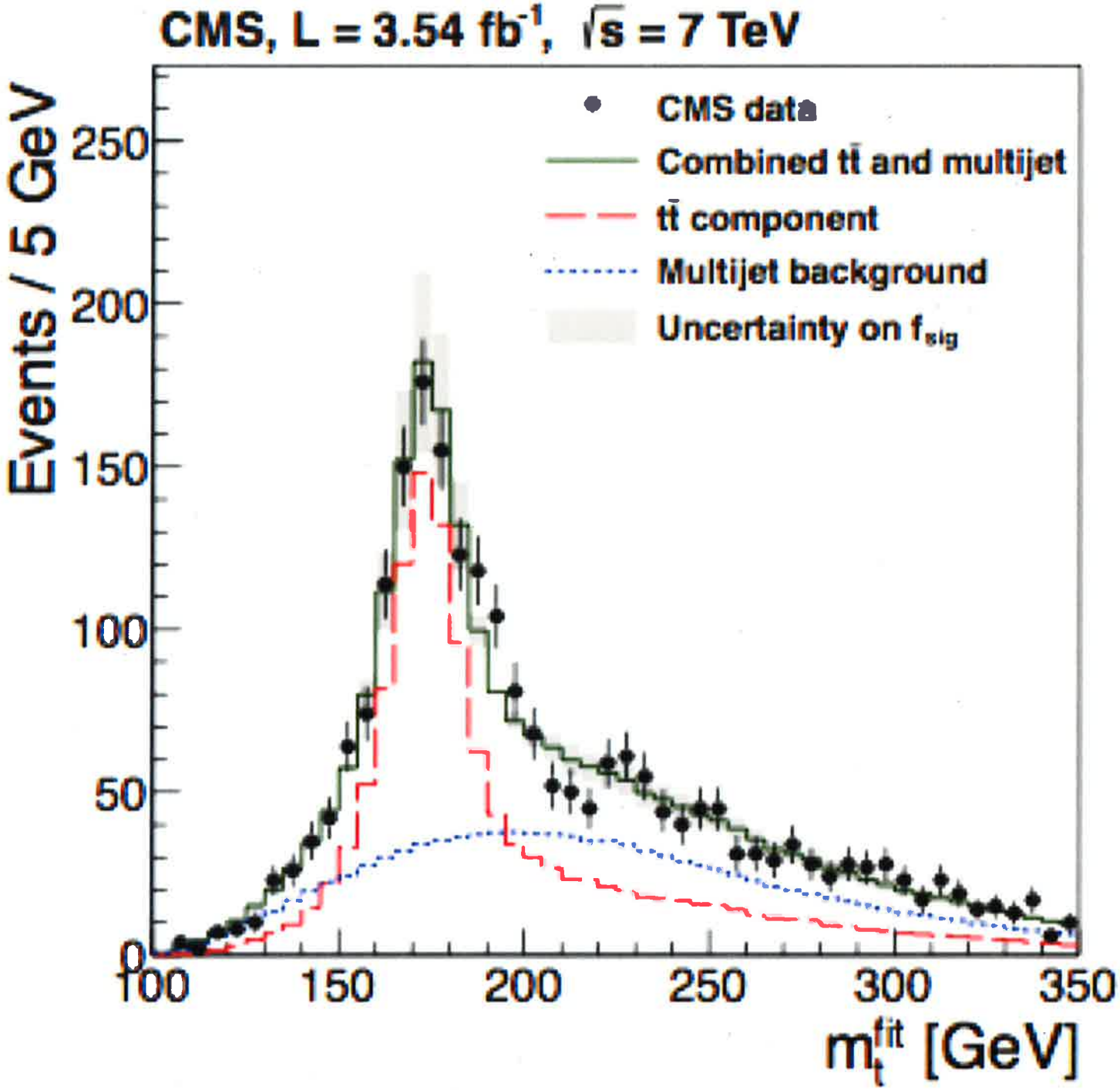

Fig. 27 Distribution of the 3-jet mass in an event sample selected for $pp \to t\bar{t} \to 6$ jets at 7 TeV, CMS Collaboration, arXiv: 1307.4617 Eur. Phys. J C74 2758 (2014)

There is one more Standard Model process that leads to leptons and $\not{E}_T$ in combination with jets. This is the single-top production process. There are two quite distinct mechanisms for producing single-top events, the t-channel process

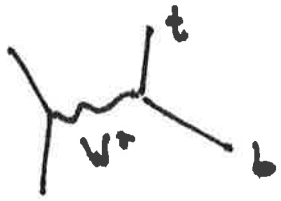

and the s-channel processd

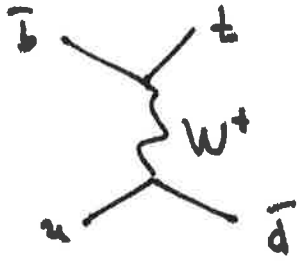

Figure 28 shows the measurement of the cross section for the t-channel process by the CMS experiment, and the comparison with the QCD expectation.

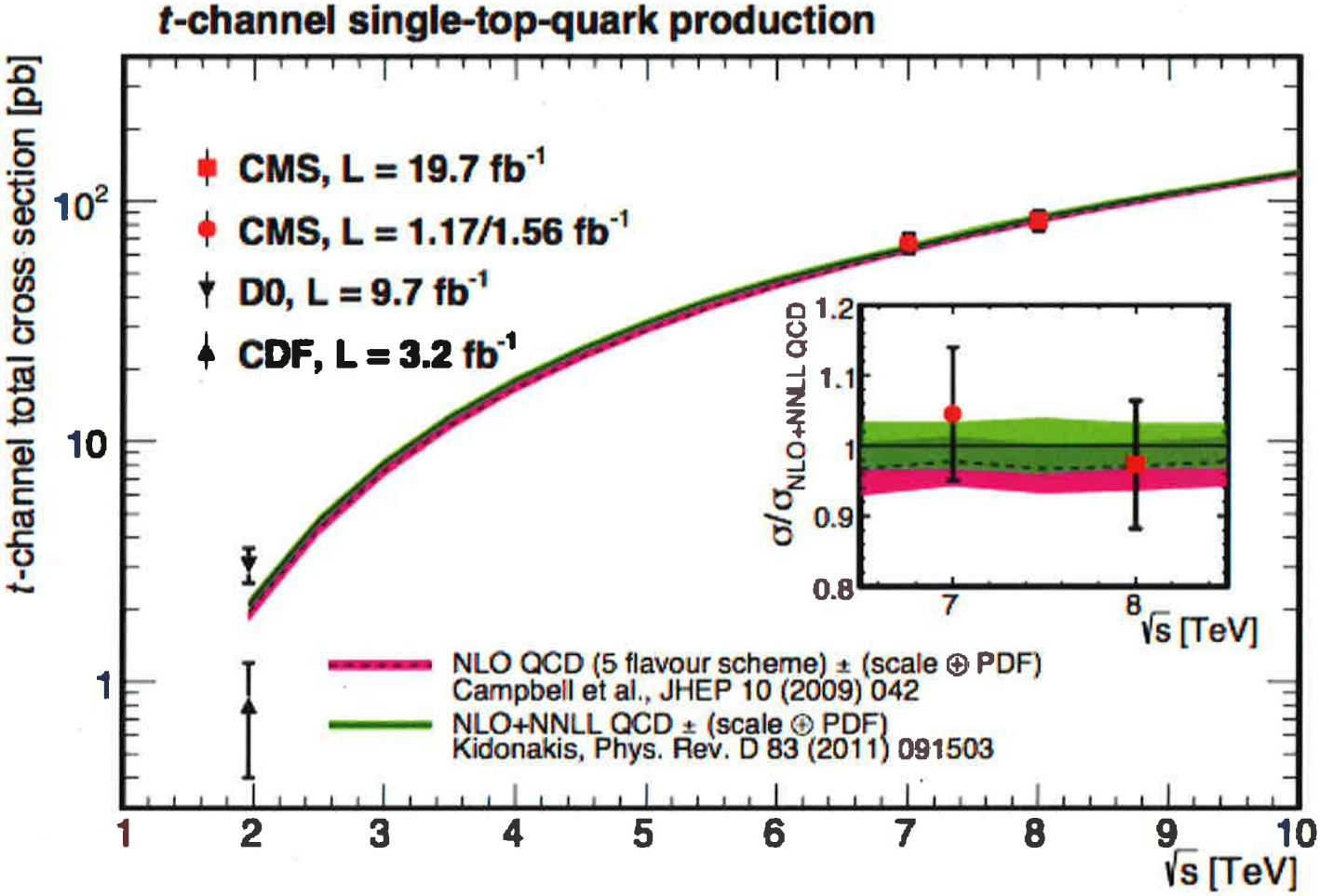

Fig. 28 Measurement of the t-channel single-top cross section at the LHC by the CMS Collaboration, arXiv: 1403.7366 JHEP 1406 090 (2014).